2011-01-01

High Temperature Oxidation Behavior Of Nb-20Si-20cr Alloys With Hafnium Additions

Alma Rosa Vazquez
University of Texas at El Paso, avazquez3@miners.utep.edu

HIGH TEMPERATURE OXIDATION BEHAVIOR OF Nb-20Si-20Cr ALLOYS WITH HAFNIUM ADDITIONS

ALMA VAZQUEZ

Department of Metallurgical and Materials Engineering

APPROVED:

_____
S.K. Varma, Ph.D., Chair

_____
Luis Trueba, Ph.D.

_____
Luis Contreras, Ph.D.

_____
Patricia D. Witherspoon, Ph.D.
Dean of the Graduate School

Dedicated to my parents, Ramon & Alma
and to my lovely husband, Christian.

HIGH TEMPERATURE OXIDATION BEHAVIOR OF Nb-20Si-20Cr ALLOYS WITH HAFNIUM ADDITIONS

by

ALMA VAZQUEZ, B.S. (MME)

THESIS

Presented to the Faculty of the Graduate School of

The University of Texas at El Paso

in Partial Fulfillment

of the Requirements

for the Degree of

MASTER OF SCIENCE

Department of Metallurgical and Materials Engineering

THE UNIVERSITY OF TEXAS AT EL PASO

May 2011

ACKNOWLEDGMENTS

I would like to thank Dr. S.K. Varma for his guidance and support throughout my master's degree, and also for giving me the opportunity to be part of his graduate research group. Furthermore, I would like to express my sincere appreciation to the members of my thesis committee, Dr. Luis Trueba and Dr. Luis Contreras for their kind advice and help. Special thanks go to Dr. Murr, who gave me the opportunity to pursue my graduate studies in the Metallurgical and Materials Engineering department. Moreover, I gratefully acknowledge the financial support of the Office of Naval Research under research program # N00014-08-1-0506, and to Dr. David Shifler who is the program manager. Finally, I greatly appreciate the encouragement of my research group and other faculty members.

ABSTRACT

Advances in aircraft and gas turbine engine technology have steadily increased the operating temperatures, and even the state of the art materials can not meet the requirements for the new challenges. Efforts are under way to study the possibility of substituting nickel-based alloys with niobium-based alloys that offer higher melting points and excellent mechanical properties. Notwithstanding these good properties, the utilization of Nb-based alloys is limited since oxidation resistant is still a serious problem. Therefore understanding the corrosion behavior of Nb-based alloys is a crucial step to enhancing oxidation resistance.

The oxidation behavior of two alloys from the Nb-Si-Cr system containing hafnium has been investigated under isothermal and cyclic conditions. Nb-20Si-20Cr-(5,10)Hf alloys (composition in atomic percent) were exposed to air for 24 and 168 hours over a range of temperatures from 700°C to 1400°C. A gravimetric method was used to determine the oxidation kinetics- weight gain per unit area as a function of temperature or time. Computed Isothermal sections of the quaternary Nb-Si-Cr-Hf phase diagrams were used for phase identification. XRD, SEM and EDS were used to characterize the phases present in the oxidation products and the alloys.

Oxidation experiments revealed extremely good oxidation resistance at 700°C and 800°C and above 1200°C under isothermal conditions for both alloys. Partial pesting was observed when the samples were exposed to 800°C. Complete oxide formation was observed at 1000°C and 1100°C for 5Hf and above 900°C up to 1200°C for 10Hf. Beneficial effects have been observed with

the addition of 10Hf to the alloy compared to 5Hf at 700°C, 1200°C and 1300°C resulting in a reduction of weight gain per unit area. Results indicate that Nb-based alloys are potential candidates for a new generation of refractory metals where microstructures and composition influence oxidation mechanisms

TABLE OF CONTENTS

LIST OF FIGURES

LIST OF TABLES

CHAPTER 1

INTRODUCTION

Requirements for high-temperature material performance have been increasing recently due to improvements in aircraft engine and gas turbine system designs. Therefore, efforts have been made towards improvements in the mechanical and oxidation properties that are crucial for alloys that are exposed to extreme corrosion environments. Lately nickel-based super alloys have been widely used in turbine-engine airfoils due to their good oxidation resistance properties and have shown outstanding performance; however, the use of these super alloys is restricted because of their relatively high density and a service temperature limit of 1,150^{o}C [1]. Then high-temperature alloys including new metallic systems that can operate at elevated service temperature above those of Ni-based super alloys are desired.

Niobium-based alloys are promising high-temperature materials exceeding 1,100^{o}C for structural applications due to the balance of properties such as high melting point (~1750^{o}C), low density (6.6 to 7.2 g/cc), and high temperature strength [2]. Nevertheless, the widespread use of Nb-based materials is still limited due to their poor oxidation resistance at elevated temperatures since the oxides that form are not protective. Therefore, extensive analyses have been made to find an excellent balance of properties by alloying Nb-Si-based alloys with chromium, hafnium, aluminum, and tin additions to create complex multiphase alloys in order to achieve the new high temperature standards. Alloying with Cr can significantly enhance the oxidation resistance by stabilizing the $NbCr_2$ Laves phase, an intermetallic compound with excellent high-temperature properties [3-11]. Other studies have been focused on the effect of the addition of small amounts of reactive elements i.e., yttrium, zirconium,

hafnium, and cerium that have a strong affinity for oxygen. Some of the reported beneficial effects of active elements to optimize oxidation behavior include improvement in the oxide adhesion and reduction in the oxidation rate, particularly for those alloys that form protective alumina scales [12-15].

The aim of this research is to study the oxidation behavior of the alloys from Nb-Cr-Si system and to determine the effect of 5 and 10 atomic percent of hafnium in a temperature range of 700-1400°C. This multiphase Nb-based alloy is of interest because of the formation of Laves phase $NbCr_2$ by the addition of Cr, niobium silicides, and Nb solid solution phases. The Nb solid solution is intended to provide tensile ductility and fracture resistance at ambient temperature. Laves and silicides are used with the purpose of providing high-temperature strength and oxidation resistance [16]. Hafnium additions are intended for improvement in both high-temperature strength and oxidation resistance, and to reduce pesting susceptibility [1,5,6]. Some physical properties of Nb, Cr, Si, and Hf are presented in Table 1.1. The results here have been presented for Nb-20Cr-20Si-5Hf and Nb-20Cr-20Si-10Hf (compositions in atomic weight percent) alloys.

Table 1.1: Physical properties of niobium, chromium, silicon, and hafnium.

Element	Atomic Number	Atomic Weight	Density at 20°C (g/cm^3)	Crystal Structure	Melting Point
Niobium	41	92.906	8.60	BCC	2467°C
Chromium	24	51.996	7.19	BCC	1860°C
Silicon	14	28.086	2.34	DC	1412°C
Hafnium	72	178.490	13.10	HCP	2227°C

The objectives include the following: determining the oxidation response and thermodynamic stability of the microstructure based on different hafnium additions. And understanding the microstructure and oxidation response based on oxidation temperature and time.

Alloy composition and oxidation temperature play an important role on the oxidation behavior. The selection of alloy composition has been chosen based on the quaternary isothermal sections of the Nb-Si-Cr system with hafnium additions at room temperature. Oxidation temperature was selected based on the limitations offered by the elements used in these Nb-based alloys. Silicon melting point (1412^{o}C) is on of the main constraints to the selection of the high temperature oxidation limits. The low temperatures were selected from 700-800^{o}C to evaluate pest behavior, which is catastrophic oxidation phenomenon observed at the low temperature regime.

The study of these factors establishes the foundation for the improvement of the oxidation resistance of Nb-based alloys.

CHAPTER 2

LITERATURE REVIEW

2.1 Oxidation - Principles

When a pure metal or an alloy is exposed to air at high temperatures it reacts with oxygen. This chemical reaction is called oxidation, and the product of the reaction is called oxide. Oxidation in air proceeds according to the following mechanisms:

1. Initial adsorption of oxygen: the oxidation process begins when the metal surface adsorbs the oxygen molecules.
2. Chemical reaction: the metal (M) reacts with the oxygen gas (O_2) to form an oxide, this oxidation reaction can be expressed as: $M_{(S)} + 1/2O_{2(g)} = MO_{(s)}$.
3. Oxide nucleation: oxides will nucleate at favorable sites and will grow and form a continuous thin oxide layer.
4. Scale growth: the thin oxide layer will continue to grow through a solid-state diffusion of the reactants through the scale to form a thicker scale. The scale then can become either a barrier between the substrate metal and the oxidizing environment and protect it from further oxidation or it may also thicken into a non-protective scale. Stresses developed during scale growth by the misfits between the oxide and metal crystals can create cavities and micro cracks that will cause the oxide to fail and spall from the metal [17-18].

2.1.1 Kinetics of Oxidation

Reaction rates are an important basis to have a better understanding about the behavior of the oxide and typically can be described as: linear, parabolic, and

logarithmic, or occasionally a combination of these. Figure 1 provides a visual demonstration of the curves where weight gain is a function of time, *t*, during oxidation process.

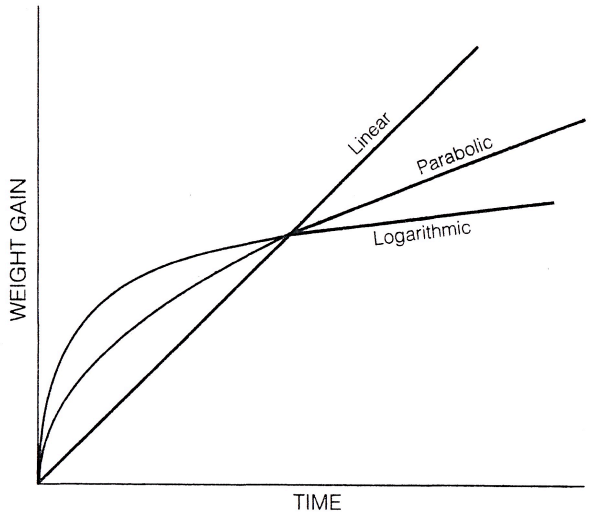

Figure 2.1: Variation of weight gain as a function of time for linear, parabolic, and logarithmic kinetic laws [20].

- Linear rate law: a constant weight gain during oxidation process has been observed when an oxide barrier does not protect the metal surface from the atmosphere. The oxidation rate remains constant with time and never slows down. After longer exposure times at high temperatures the metal will continue to oxidize until it is completely destroyed. This reaction is controlled by surface diffusion and adsorption mechanisms. The linear rate equation is represented as:

$$dx/dt = k_L \text{ or } x = k_L t \tag{2.1}$$

Where x is the mass or thickness of oxide formed, t is the time of oxidation, and k_L is the linear rate constant.

- Parabolic rate law: metals and alloys frequently exhibit this oxidation behavior at high temperatures and are controlled by the diffusion process. During the oxidation process the ions are diffused through the oxide scale and as the oxide layer increases the diffusion distance increases, and the oxidation rate slows down. Therefore, the rate of the reaction is inversely proportional to the scale thickness. This is represented as:

$$\frac{dx}{dt} = \frac{k_P}{x} \text{ or } x^2 = \frac{k_P}{2}\, t \quad (2.2)$$

Where k_P is the parabolic rate constant.

- Logarithmic rate law: the initial oxide formation is characterized by an initial rapid response that promptly reduces to a low rate of reaction. Often at lower temperatures, the oxidation rate is inversely proportional to time, t. The kinetic law is either direct logarithmic or inverse logarithmic kinetics type:

Logarithmic equation where k_e and a are constants: $x = k_e \log(at + 1)$ (2.3)

Inverse logarithmic equation where b and k_i are constants: $\frac{1}{x} = b - k_i \log(t)$ (2.4)

Adsorption and transport of ions through oxide film have been assumed to be the rate-determining process during early oxide-film formation. [17, 19,20]

2.1.2 Protective Oxides and Protection Failure

Oxidation resistance has been the most challenging obstacle to the expansion of the uses of Nb-based alloys for high temperature applications since it reduces their high-temperature service life. Therefore, some research efforts have been directed toward alloy design to create protective oxide scales to withstand degradation [21]. There are two essential requirements: first, the protective oxide should be compact and perfectly adhere to the metal substrate under all conditions, and secondly this layer

should thicken at a slow rate into the metal [22]. Alloys exposed to high temperature rely upon the oxidation reaction to develop a protective oxide layer that should be chemically and mechanically stable to prevent further oxidation. Oxides that form protective oxide layers that are thermodynamically stable are Cr_2O_3, alumina (Al_2O_3), and silicon dioxide (SiO_2).

Studies have concentrated on the use of aluminum to enhance oxidation resistance of different Nb-based alloys through the formation of a protective alumina layer. It has been reported that aluminum in the $Nb_3Si_5Al_2$ matrix compacts improved the oxidation resistance at ~1,300^oC due to the formation of a thin adherent Al_2O_3 layer [23-26]. The addition of Cr can play an important role in enhancing the oxidation resistance due to the formation of Cr_2O_3 oxide protective scale, however, this oxide is limited to below about 1,000-1100^oC. At higher temperatures Cr_2O_3 dissociates into volatile CrO_3 [18, 24, 27-29]. The addition of silicon content could result in the formation of amorphous silica (SiO_2) that is very protective and can decrease the oxidation rate. Even though SiO_2 is thermodynamically more stable than Cr_2O_3, the mobility of silicon is much lower than Cr and the SiO_2 rarely forms on alloys via oxidation. Moreover, in high temperature regions SiO_2 layers also are volatilized [18, 27, 29]. Besides volatilization, spallation of protective oxides is also a common issue encountered in alloy design. Spallation is a common cause of failure of protective scales due to stresses created by cooling from the reaction temperature. These stresses generate due to the difference in the coefficients of thermal expansion between the metal and the oxide [17].

2.2 Refractory Metal Intermetallic Composites

Refractory metals (i.e. niobium, molybdenum, and tantalum) have high-melting temperatures (above 1925^{o}C), and are subsequently suitable for high-temperature applications. However, the use of refractory metals is limited due to their poor high-temperature oxidation resistance since these metals begin to oxidize between 200^{o}C and 425^{o}C. Of all the refractory metals, with a melting point of 2467^{o}C, niobium is the most promising based alloy for structural applications due to its exceptional properties. However, during oxidation the surface layer of niobium pentoxide forms and is not protective because it cracks and spalls. Therefore alloying of Nb refractory metals with different elements is a good way to extent its high temperature service capability.

2.2.1 Niobium-Silicon System

Among different refractory-metal intermetallic composites (RMICs) niobium-silicide-based composites offer excellent mechanical and physical properties at high- and low temperatures. Metal silicide composites posses increased temperature capability, reduced density, high strength, and high stiffness [30]. The equilibrium phase diagram of the Nb-Si binary system in Figure 2.2 shows the liquidus phase, two solid solutions (Nb) and (Si), and the existence of three intermetallic compounds: Nb_3Si, Nb_5Si_3, and $NbSi_2$. The Nb_5Si_3 (5-3 silicide) phase has the highest melting point (2515^{o}C) and exists in two tetragonal modifications, α-Nb_5Si_3 from room temperature to 1935^{o}C and β-Nb_5Si_3 from 1642^{o}C up to 2515^{o}C. The difference in their crystal structure is their lattice parameters (nm): β-Nb_5Si_3 $a=1.0040$ and $c=0.581\ (\mathrm{nm})$, and for α-Nb_5Si_3 $a=0.6571$ and $c=1.1889$ [31]. Melting point of $NbSi_2$ with a hexagonal structure is 1935^{o}C. The Nb_3Si has a tetragonal structure. The Nb_3Si is only stable between 1700^{o}C

and 1975°C, and below 1700°C experiences eutectoid decomposition to Nb and α-Nb_5Si_3. A peritectoid reaction occurs at 1948°C Nb_3Si + β- Nb_5Si_3 ↔ α- Nb_5Si_3 and eutectoid reaction occurs at 1642°C β-Nb_5Si_3 ↔ α- Nb_5Si_3 + $NbSi_2$.

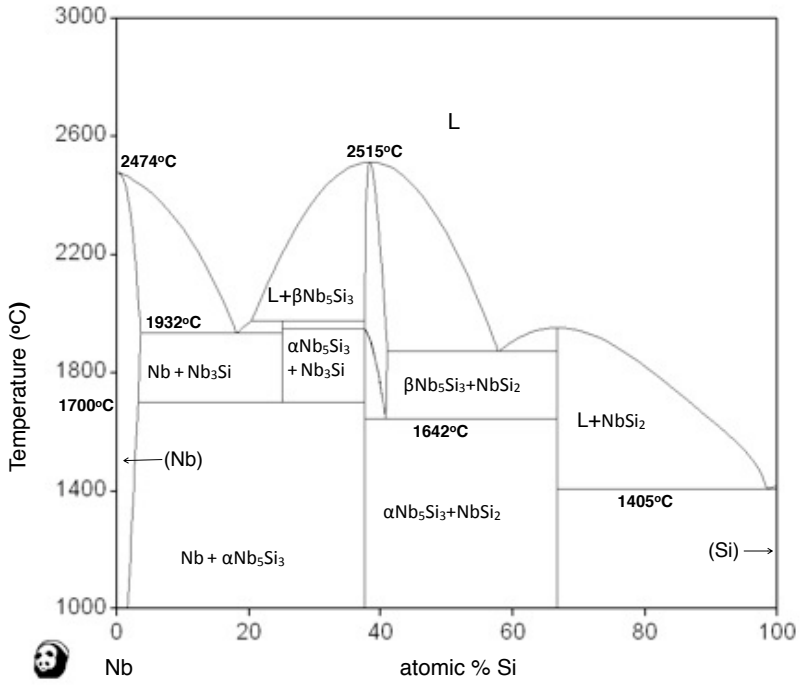

Figure 2.2: Binary phase diagram for Nb-Si alloy system calculated by Pandat™ software [48].

Niobium-silicide-based composites typically have Si content ranging from 10 to 25 at.% in which microstructures often comprise a metallic solid solution phase (β) embedded in a matrix of intermetallic compounds including: Nb_5Si_3, Nb_3Si, or a mixture of both [2-4, 8]. However, the microstructure of the niobium-silicide based composite varies according to the alloy composition. In a recent study, Geng et al. [3] reported that the addition of titanium to Nb-Si-Cr-Al-Mo system stabilizes the β-Nb_5Si_3 to lower temperatures (at least to 1300°C). Similar behavior has been observed with the addition of 6 at.% aluminum to a Nb-16Si in which the presence of β-Nb_5Si_3 phase was evident, suggesting that Al promotes the direct formation of this phase [32]. Other authors have

reported the presence of a new niobium silicide phase with the addition of hafnium to Nb-Si-Ti-Al and Nb-Si-Cr-Al-Mo systems. This phase has been identified as γ-Nb_5Si_3 with a hexagonal $D8_8$ structure with lattice parameters of $a=0.7536$ and $c=0.5248$ (nm). This phase has been treated as an impurity phase and has not been included in the Nb-Si binary phase diagram because its formation mechanism has not been clear at present [3,32].

2.2.2 Niobium-Chromium System

Among many Laves phases intermetallic compounds of the form XCr_2 are particularly attractive for high temperature applications since chromium is an important alloying element for improving oxidation resistance due to its high melting point (1860^{o}C) and low density (7.19 g/cm^3). Cr combined with Nb refractory metal can form $NbCr_2$ type Laves phase with excellent properties such as for high temperature applications due to its high melting point (1730^{o}C), relatively low density (7.7 g/cm^3), good creep resistance, high strength, and good oxidation resistance (below 1100^{o}C). Intermetallic compounds with the composition AB_2 can crystallize into Laves phases, which exist in three structure types: cubic $MgCu_2$ (C15), hexagonal $MgZn_2$ (C14), and hexagonal $MgNi_2$ (C36) [33]. The difference between C14 and C36 Laves phases is the lattice parameter in their crystal structure. The lattice parameters of C14 is $a=4.976$ and $c=8.059$, and for C36 is $a=4.98$ and $c=16.12$ (nm). The assessed Nb-Cr phase diagram is shown in Figure 3. The high temperature form of Laves phase (C14) is stable above 1650^{o}C while the low temperature form of Laves phase (C15) is stable at temperatures below 1650^{o}C. However, it has been reported that silicon promotes the formation of C14 Laves phase and stabilizes it at lower temperatures [31,34].

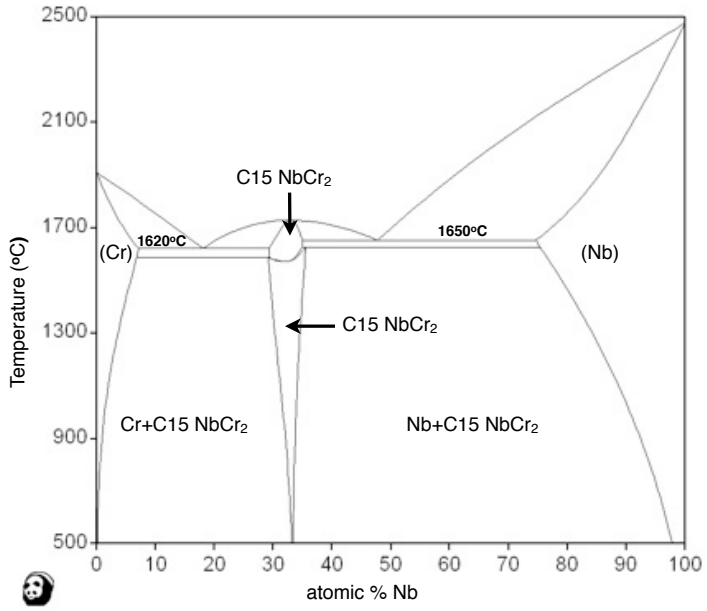

Figure 2.3: Binary phase diagram for Nb-Cr alloy system calculated by Pandat^{TM} software [48].

2.2.3 Niobium-Silicon-Chromium System

Promising refractory metal composites need an excellent balance of mechanical properties at low and high temperatures, metals with good ductility that can provide room temperature fracture toughness and intermetallics that exist in equilibrium with metals that can provide strength at high temperatures. Among these, niobium solid solutions and niobium silicides are of interest due to their high strength and high melting temperatures, however, despite their outstanding properties they have poor oxidation resistance. Therefore, Cr is often added to enhance oxidation behavior due to stabilization of the $NbCr_2$ Laves phases. Depending on the alloy composition, different silicides, modifications of Laves phases (C14 and C15), and metallic solid solution phase can be present in the microstructure of Nb-based alloys. It has been reported that Nb-Si-Cr alloys containing 12-30 at.% Si and 8-45 at.% Cr generally comprise 3-1 and 5-3 silicides, C14 Laves phase, and Nb_{ss} [35-36]. The metallic solid solution phase is

ductile at room temperature, has low density and it provides the majority of the toughness [2,4]. The silicon concentration controls the volume fraction of silicide, and thus it is important for the elevated temperature strength and creep properties, where Nb_5Si_3 is preferred for higher creep resistance owing to its higher melting temperature [1].

2.3 Niobium-Oxygen System

The study on the temperature dependence of the oxidation of pure niobium has been of great interest since it would reveal oxide formation and behavior. Niobium with a typical metallic bcc structure forms several oxides but none of them protect the metal from further oxidation. The main oxides that form are NbO, NbO_2, and several polymeric forms of Nb_2O_5, the last oxide being the most stable. The oxidation mechanism of niobium can be described initially by the formation of a protective layer followed by scale cracking and breakaway of the oxide scale. During the initial stages the oxidation occurs with the dissolution of oxygen in the metal and formation of metastable oxides. Then, reaction mechanisms change above 650^{o}C where NbO or NbO_2 develops directly from the solid solution of the oxygen and niobium rather than metastable oxide forms at lower temperatures. Breakaway of the oxide has been associated with the formation of Nb_2O_5 [18, 19]. Sheasby [37, 38] in two different studies observed that oxygen is the most moveable species during the oxidation of niobium. Hurlen [39] observed several oxidation stages for pure niobium over large ranges of temperature and oxygen pressures. The time dependence indicates the following sequential oxidation stages in a temperature range of 150-1000^{o}C: linear (I), parabolic (II), a rate-increasing transition (a

transition from a protective to a non-protective type of oxidation), linear (III), parabolic (IV), and parabolic (V).

Brauer [40] identified three modifications of niobium pentoxide and identified them according to the temperature in which the oxides formed. Orthorhombic modification T-Nb_2O_5 exists at low temperatures below 900^oC, whereas the monoclinic M-Nb_2O_5 appears at a temperature above 900^oC and the high temperature monoclinic H-Nb_2O_5 that develops at a temperature above 1100^oC. Holtzberg re-designated them as γ-T, β-M and α-H and reported an irreversible phase transition from γ to α-Nb_2O_5 at ~830^oC with a volume increase of ~13.5%. Waring et al. [51] observed a base-centered monoclinic modification of niobium pentoxide formed at 900^oC. Arbuzov et al. [41] observed a phase transformation α→ β-Nb_2O_5 at 850^oC, where both modifications were observed with orthorhombic crystal structure but with an increase in the lattice constant nearly twice as large, with about 11% increased in volume. Goldschmidt [42] performed an investigation on the phase transformation of niobium pentoxide and found two modifications; a metastable low temperature α-Nb_2O_5 that transforms to a high temperature β-Nb_2O_5. The stabilization of alpha and beta modifications of Nb_2O_5 can be achieved with additions of certain oxides of other metals. For instance, it has been found that silica is an alpha- Nb_2O_5 stabilizer.

2.4 Oxidation of Nb-based Alloys and Alloying Effect

Extensive research has been done to enhance the oxidation resistance of niobium-based alloys for high-temperature applications. Bewlay et al. [6] outline the role of silicon as beneficial on high temperature alloys with promising results at temperatures above 1000^oC and comparable to that of Ni-based super alloys, followed by Cr and Ti.

Simple composites are based on binary Nb-Si alloys, but more complex alloys are created when alloyed with Cr, Hf, Ti, Sn and Al. Nb-Si-Cr systems have been studied in detail since it provides a basis for the development of new corrosion resistant alloys. Recent efforts have focused mostly on multi-phase alloys containing an appropriate mixture of niobium solid solution, niobium silicides and Laves phases [35,43]. It was observed that Cr concentration had a significant effect on the oxidation behavior, and that oxidation resistance increased with the elevation of the Cr content. The Nb_5Si_3 phase played a significant barrier against the outward diffusion of Cr during the oxidation process. Then, reducing the volume fraction of Nb_5Si_3 phase favors the formation of $CrNbO_4$. The effects on minor additions such as aluminum and tantalum have also been investigated [25]. The Nb-Ti-Si system with Al and Ta exhibited linear oxidation kinetics, however, the highest oxidation rate was observed with no alloying additions and complete disintegration into powder. This suggests that Al and Ta additions were beneficial in suppressing pesting behavior. Nb-Ti-Si with Al addition was observed with the lowest weight gain rate, while Ta additions promoted a higher rate and lower oxide scale adhesion. Al additions promoted the formation of $AlNbO_4$, while Ta the Ta_2O_5 oxide.

The cyclic oxidation response of niobium-based alloys with various compositions (Nb, Ti, Hf, Cr, Ge, and Si) has been studied by Chan in a temperature range of 900-1400^{o}C [8]. Additions were intended to retard oxidation kinetics and to modify the oxidation products. Results indicate that Nb solid solution phase oxidized selectively, while the silicide phase did not. The oxidation resistance of intermetallic compounds was determined by the nature of the oxide products that form on the surface. At 1400^{o}C the alloys showed poor oxidation resistance with oxide products containing mostly

Nb_2O_5 and $Nb_2O_5{\cdot}TiO_2$ with little $CrNbO_4$. The oxidation resistance of the Nb-based alloys was enhanced by the formation of $CrNbO_4$ instead of a combination of oxides including Nb_2O_5, $Ti_2Nb_{10}O_{29}$, and Nb_2O_5-TiO_2, and by alloys whose microstructure consisted of Nb-based silicides and Laves phase, with minimum of Nb_{ss} phase. The formation of continuous SiO_2 on Nb-based alloys was difficult due to low solubility of Si on Nb.

Recent work has explored the Nb-Mo-Si-B system where Nb and Mo are expected to substitute for each other [44]. At 800°C the alloys suffered catastrophic oxidation, and high oxidation rate at 1200°C. Moreover, mass change process was observed during oxidation mass gain due to the oxidation of Nb, Si, and B, and mass loss due to the volatilization of MoO_3. A different oxidation behavior occurred when titanium was added to Nb-Mo-Si-B system [45]. A linear oxidation behavior has been observed at 800°C with a porous oxide scale, and parabolic oxidation behavior at 1300°C with a scale containing layered structure composed of Mo oxides, Nb_2O_5, and TiO_2 in a SiO_2 matrix. Recent efforts have focused to determine the effect of the addition of various alloying elements on the oxidation behavior. The effect of alloying titanium on the oxidation behavior has been reported in Nb-Si-Al, Nb-Si-Cr-Al, and Nb-Si-Cr-Al-Mo systems between 800 and 1200°C [3,9,11]. The addition of Ti increased the oxidation resistance of the alloys, and suppressed the formation of the Laves phase in the Nb-Si-Cr-Al and Nb-Si-Cr-Al-Mo systems.

At intermediate temperatures (T<850°C) refractory metals are vulnerable to pesting damage. Pesting is the term that is often used to describe a dramatic oxidation phenomenon observed in intermetallic alloys that leads to disintegration of a susceptible compound into powder [1,2,9,46] However, other authors have suggested that it occurs

due to intergranular diffusion of oxygen and the formation of oxides within the grains that create high internal stresses [25]. According to Bewlay et al. [1] Al and Hf additions can help to reduce the pesting behavior of Nb-based alloys. J. Geng and P. Tsakiropoulos [3] reported pest oxidation behavior in the Nb-Ti-Si-Cr-Al-Mo system with 5Hf addition at 800^{o}C that was eliminated with the addition of 5Sn to the system. Suggesting that Sn in the Nb-silicide based composite played a crucial role in suppressing the pest oxidation phenomenon of the system at intermediate temperatures.

Besides titanium and tin additions, hafnium is an important alloying element used in various heat-resistant alloys. Hafnium is an oxygen-active element and will never form a protective oxide scale but can improve the oxidation resistance due to the high solubility of oxygen in hafnium at elevated temperatures. It has been reported that Hf addition reduces oxygen solubility and diffusivity in the alloys [25,47]. J. Geng et al. [9] have studied the oxidation of Nb-Si-Cr-Al system that showed inferior oxidation resistance compared to Ni-based super alloys. The research consisted of using different alloying elements and studying the effects on the oxidation behavior. Even though the addition of Hf did not change the oxidation kinetics at 800°C it reduced the oxidation rate at 1200°C. The study would suggest that Hf might play a more important role in the oxidation of the alloys at 1200^{o}C compared to 800^{o}C. Hafnium can be added to the alloys either in elemental form or as hafnium oxide dispersoid (hafnia). Several authors have reported hafnia in the as-received condition of the alloys [3,4,9]. Because Nb has high oxygen solubility, it needs to be alloyed with an element that increases its performance either by promoting the formation of a protective oxide or an element that

will oxidize preferentially. Small additions of elements with high affinity of oxygen (active elements) are known to be very effective to mitigate this problem [21].

CHAPTER 3

EXPERIMENTAL DETAILS

3.1 Alloy Fabrication

The Ames Laboratory located at the Iowa State University fabricated the Nb-based alloys used for this study via the arc melting technique under a high purity argon atmosphere. The elements were metallurgical grade with 99.95% purity with the exception of the Si, which was 99.999%. After casting, the ingots were remelted several times to ensure homogeneity and were electrically discharged machined (EDM) into 5 x 5 x 5 mm samples squares. Alloy composition used for this study is listed in Table 3.1 in atomic percent.

Table 3.1 Alloy composition in atomic percent.

Element	Nb (at%)	Si (at%)	Cr (at%)	Hf (at%)
5Hf alloy	55	20	20	5
10Hf alloy	50	20	20	10

3.2 Oxidation Experiments

The as-received alloys were prepared for oxidation experiments by the following steps:

1. Before testing, all major surfaces were polished down to a 600-grit SiC paper in order to remove any initial oxide layer.
2. Dimensions of the samples were measured using a micrometer to an accuracy of 0.01mm to obtain the total surface area that was going to be exposed to high temperatures.

3. The samples were ultrasonically cleaned for fifteen minutes in ethanol to remove the particles adhered to the alloy.
4. The silica based (SiO_2) Leco 528 HP crucibles and caps used for the oxidation experiments were furnace dried at 300°C for two hours in order to remove any moisture.
5. The samples were placed in the dried crucibles with a cap on top to prevent material loss during the oxidation process.
6. Initial and final weight of the sample and crucible were monitored using a Sartorius Analytical balance (Model MC210S) with an accuracy of six decimal places.

Oxidation kinetics of both alloys were studied in static air in a temperature range of 700 to 1400°C using programmable furnaces (Sentro Tech ST-1600-888). Two oxidation studies were performed: short term oxidation (STO) and long-term oxidation (LTO).

3.2.1 Isothermal Oxidation

Isothermal oxidation experiments were undertaken from 700-1400^{o}C. The samples were exposed to the desired temperature for 24 hours at a heating rate of 10°C/min followed by furnace cooling to room temperature. The purpose of this experiment was to predict how the alloy would behave in its first hours of service. After each oxidation experiment, the recorded data for weight changes were plotted as weight gain per unit surface area as a function of temperature to determine the oxidation kinetics

3.2.2 Cyclic Oxidation

Cyclic oxidation experiments consisted of heating the samples to the oxidation temperature, which ranged from 700-1400^{o}C. The samples were held at the temperature for 24 hours and then furnace cooled to ambient temperature. The specimens were weighed before and after each heat treatment. This process was repeated seven times for a total oxidation time of 168 hours. The weight changes were plotted as weight change per unit surface area as a function of time. The oxide spalls were collected in glass vials for individual alloys for analysis.

3.3 Characterization of Alloys and Oxide Products

The as-received alloys and oxidation products were characterized using scanning electron microscope (SEM) with an energy dispersive x-ray spectrometer (EDS), x-ray mapping, and x-ray diffraction (XRD).

As-cast specimens were ground with silicon carbide papers up to 1200 grit then further polished using felt cloth and alumina 1μm, 0.3μm and 0.5μm slurries for characterization. Oxidized samples were mounted in an epoxy resin and ground with silicon carbide papers to 1200 grit finish. Before SEM analysis the samples were sputter coated with gold using a SPI-MODULE to avoid any charging effects.

The surface morphologies of the alloys and cross section of the scales were analyzed by SEM, most of the times by secondary electron and backscatter electron mode using Hitachi S-4800 (FESEM). EDS analysis was used to identify the elemental composition of the phases present in the metal and oxide scale. X-ray mapping was used to detect the elements present in the alloys. SEM and EDS analysis were performed under the following operating conditions:

- Accelerating voltage: 20KV
- Probe current: 20μA
- Working distance: 7-16 mm
- EDAX 5.21 Genesis Imaging, Mapping Software
- Dwell time: 30 sec

X-ray diffraction (XRD) was used to identify the phases present in the alloys and the oxidation products. A XRD machine (Bruker D8 Discover) was used with monochromatic Cu Kα radiation (λ=1.540562 Å). The oxidation products were pulverized until a fine powder was obtained previous to x-ray analysis. The XRD analysis was performed under the following operating conditions:

- Voltage: 40KV
- Current: 40mA
- Step: 0.05^{o}
- Scan rate: 5^{o}/min
- Divergence slit: 0.2 mm
- Scatter slit: 8mm

3.4 Phase Diagram Calculation

Isothermal sections for the Nb-Si-Cr-Hf quaternary system were calculated using a phase diagram calculation software for multicomponent systems, PANDAT^{TM} 8.2 by CompuTherm. Calculating the isothermal sections was for alloy selection purposes and to provide information such as phases with their crystal structure based on the compositions.

CHAPTER 4

RESULTS AND DISCUSSION

4.1 Isothermal Sections from Nb-Si-Cr System with Hf Additions

Calculated isothermal sections using Pandat^{TM} 8.2 software for 5 and 10 hafnium alloys are shown in figure 4.1. Phase diagrams and related thermodynamic information are fundamental to understand the thermodynamic properties and phase stability of the alloys. Isothermal sections for the Nb-Si-Cr-Hf quaternary system were calculated based on the Nb-Si-Cr ternary system with 5 and 10 Hf atomic percent fixed concentrations. The quaternary system at room temperature for Nb-20Cr-20Si-5Hf alloy indicates the presence of solid solution (α), $Nb_9Si_2Cr_3$ (9-2-3 silicide) and hexagonal C-14 Laves phase ($NbCr_2$). With the addition of 10Hf to the Nb-20Cr-20Si alloy a new silicide Hf_2Si is added to the system.

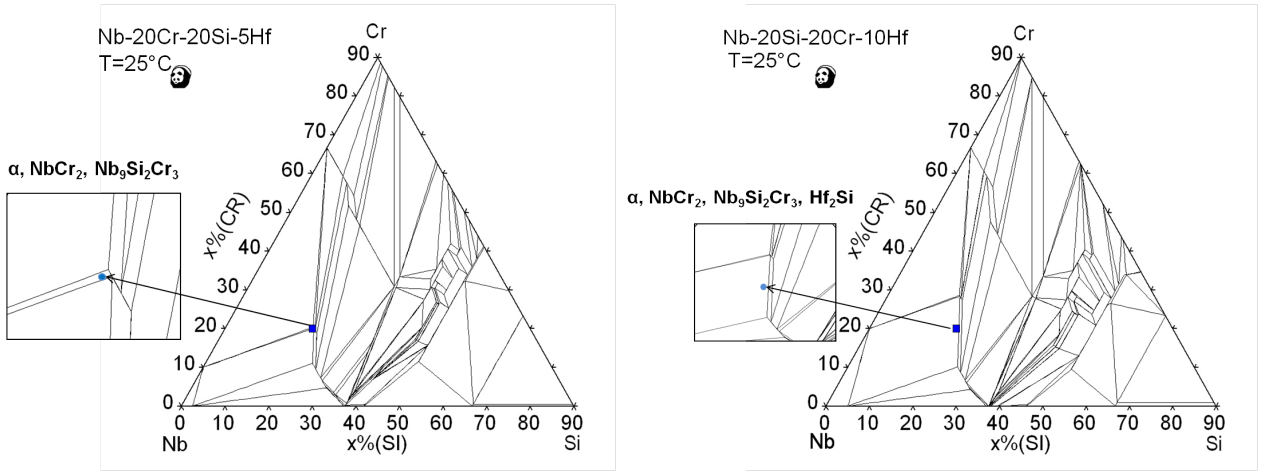

Figure 4.1 Isothermal Sections for Nb-Cr-Si-Hf system at room temperature.

4.2 As-cast Characterization

4.2.1 Scanning Electron Microscopy, SEM

Backscatter (BSE) images for 5Hf and 10Hf alloys in the as-cast condition are presented in Figure 4.2. The microstructure consists of Nb_5Si_3 (5-3 silicide, gray) and $NbCr_2$ (dark gray). In addition, there is a region that appears to be eutectic-like and consists of three phases: solid solution (α, light gray), Laves (dark gray) and 5-3 silicide (gray) phases. The alloys also contain a white microconstituent present in the backscatter images that appears to be Hf rich phases. The average composition of the precipitates was determined by elemental analysis to be 40.03at% Hf, 1.81at% Cr, and 58.16at% O confirming that these white phases are HfO_2. The silicon element was omitted from the EDS spectrum of the white phase for a more accurate analysis since the peaks of Hf-M (1.645eV) and Si-K_α (1.740) almost overlap. However based on EDS analysis it was confirmed that there was a small amount of silicon in the white phases (HfO_2). The formation of hafnia in the sample is easy to understand considering the high stability of this oxide. In addition to the four phases, 5-3 silicide and Laves phases rich in hafnium resulted in lighter contrast under BSE imaging conditions. The average composition for 5Hf alloy was 52.29at.% niobium, 20.44at.% silicon, 22.16at.% chromium, and 5.11at.% hafnium. While the average composition for 10Hf alloy was 48.26at.% niobium, 21.15at.% silicon, 20.06at.% chromium, and 10.53at.% hafnium. Figure 4.3 shows the elemental x-ray mapping of the 5Hf alloy. The intensity of the color, and color distribution is related with the concentration and distribution of each element. It shows that silicon is mostly concentrated in the primary silicides and secondary silicides in the eutectic-like area as expected, but little concentration in the Laves phases. However, chromium is highly concentrated in the Laves phases but

minimum concentration in the Nb_5Si_3 phase. On the contrary, hafnium appears highly concentrated in the hafnia phase and almost equally distributed within the other phases. Chromium concentration in the α phase appears to be higher with 13.77 at% compared to silicon and hafnium, with 2.31 at% and 6.29 at% respectively for 5Hf alloy. Similar compositions were observed in the α phase for 10Hf alloy with 10.55 at% silicon, 4.03 at% hafnium and 6.32 at% silicon.

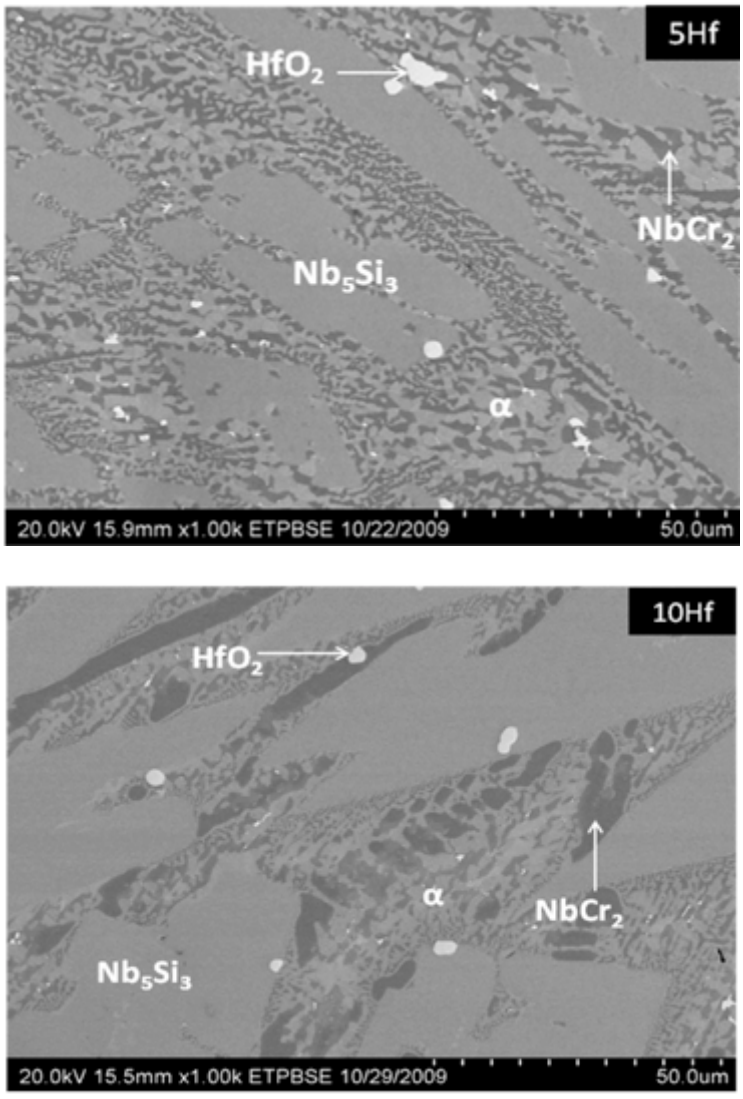

Figure 4.2. As-cast microstructure of 5Hf and 10Hf alloys.

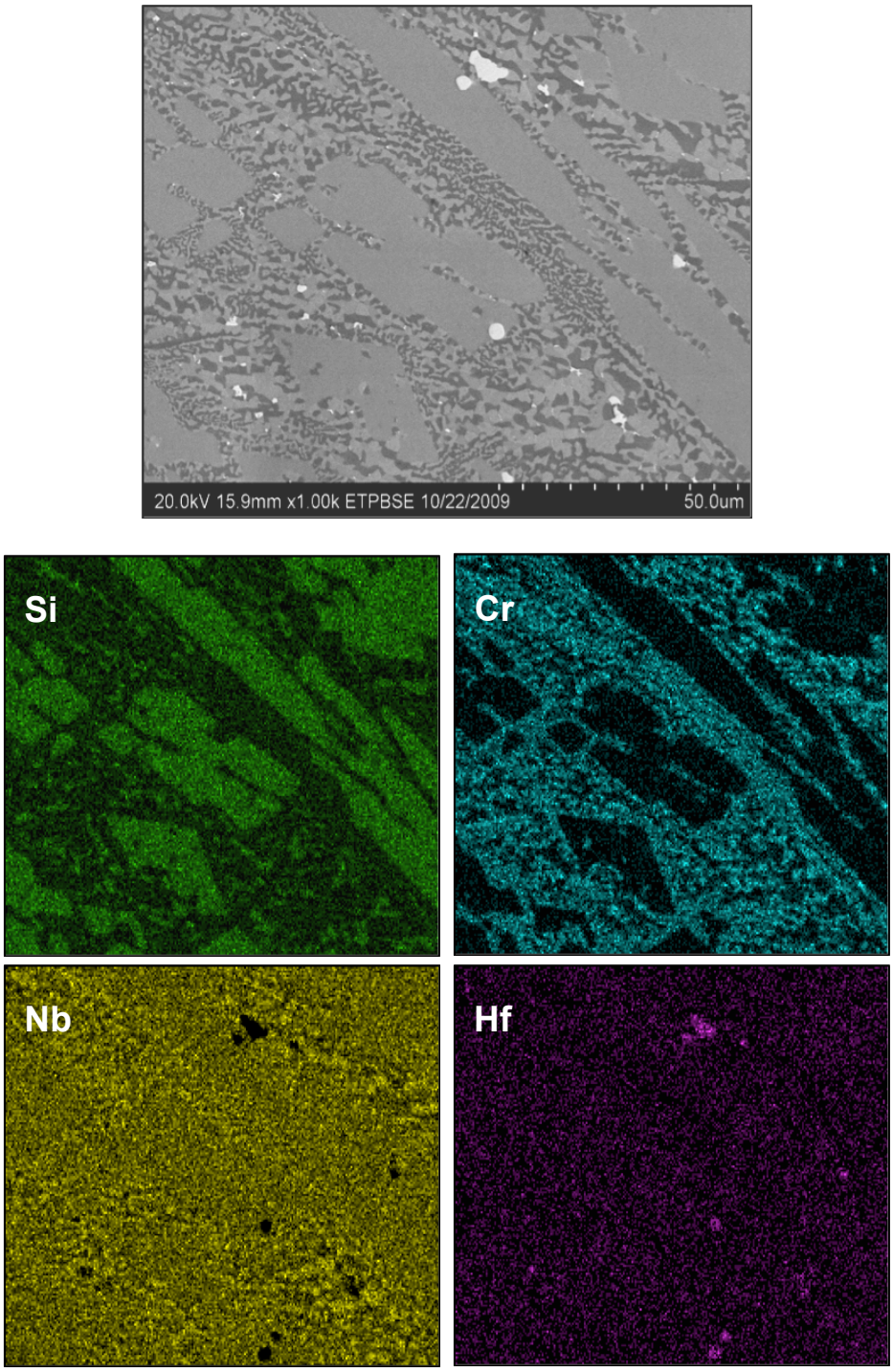

Figure 4.3. X-ray mapping on the 5Hf as cast alloy microstructure of Si, Cr, Nb, and Hf.

4.2.2 X-ray Diffraction, XRD

The XRD spectrum obtained from the as-cast Nb-20Cr-20Si-5Hf and Nb-20Cr-20Si-10Hf alloys are shown in Figures 4.4 and 4.5 in which each phase was identified as well as the crystal structure. The presence of four phases was confirmed, α with a body center cubic (BCC) structure, $NbCr_2$ (C14) with a hexagonal structure. As well as two modifications of the Nb_5Si_3 phase (α and β) were detected with a tetragonal crystal structure. The peaks of α solid solution phase appear to be shifted to the right for less than a degree, this can be attributed to the alteration of the niobium lattice due to the alloying elements that are going into the phase in the form of solid solution. Unfortunately, the X-ray diffraction machine could not detect hafnia phase and the possible reason for this is that there was little amount of hafnium to be detected.

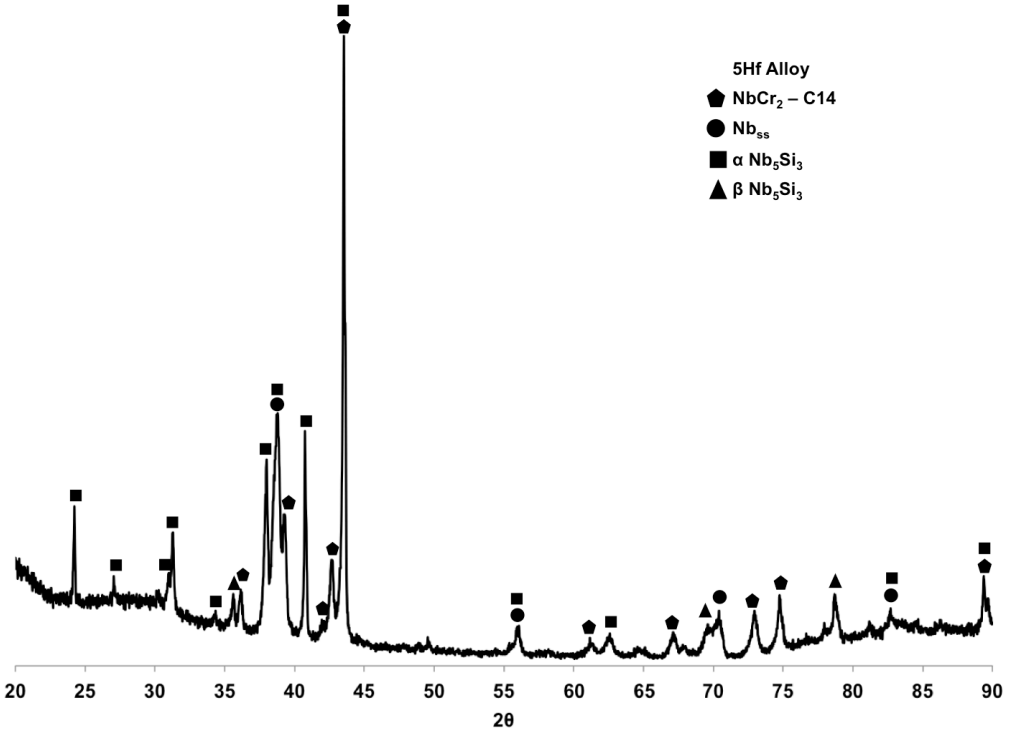

Figure 4.4. XRD pattern of 5Hf alloy in the as-cast condition.

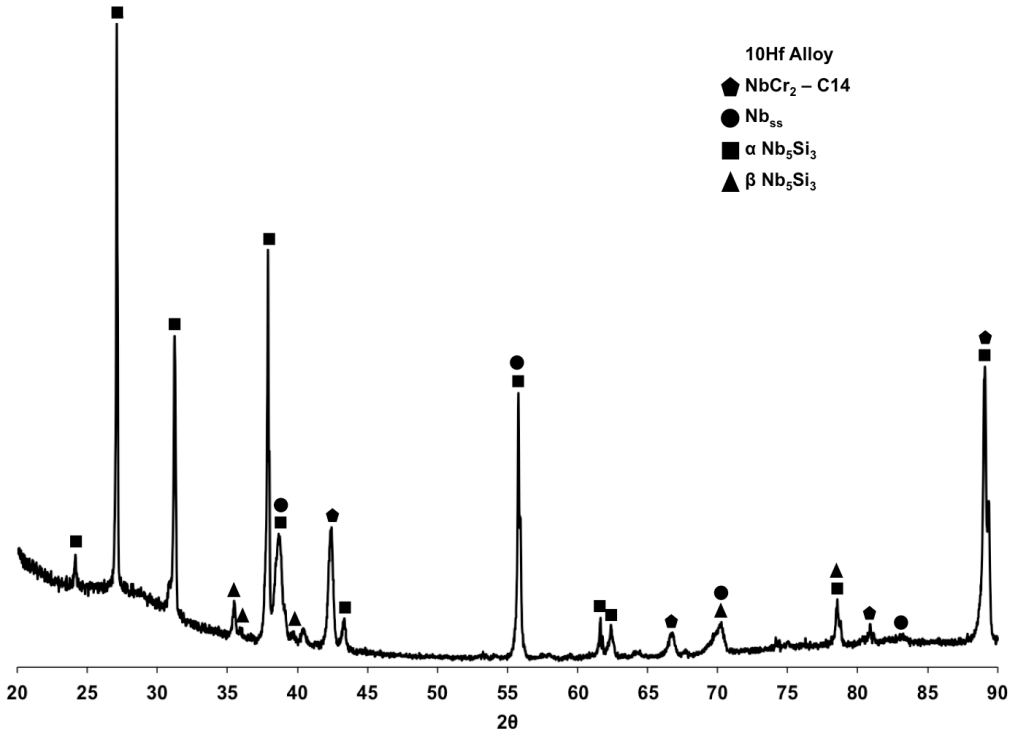

Figure 4.5. XRD pattern of 10Hf alloy in the as-cast condition.

4.3 Isothermal Oxidation

4.3.1 Oxidation Kinetics

Figure 4.6 shows the isothermal oxidation curves for 5Hf and 10Hf alloys obtained at temperatures ranging from 700°C-1400°C. This curve represents weight gain per unit area as a function of oxidation temperature, which also indicates the condition of the samples after the oxidation test (●-fine powder oxide scale, ▲-thin oxide scale, and ■-bulky oxide scale). Similar oxidation resistance as well as oxidized products has been observed for both alloys. The oxidation response can be explained in three different stages according to their weight gain per unit area and oxidation products. Figure 4.7 shows the morphology of the oxidation products for 5Hf alloy for visual reference.

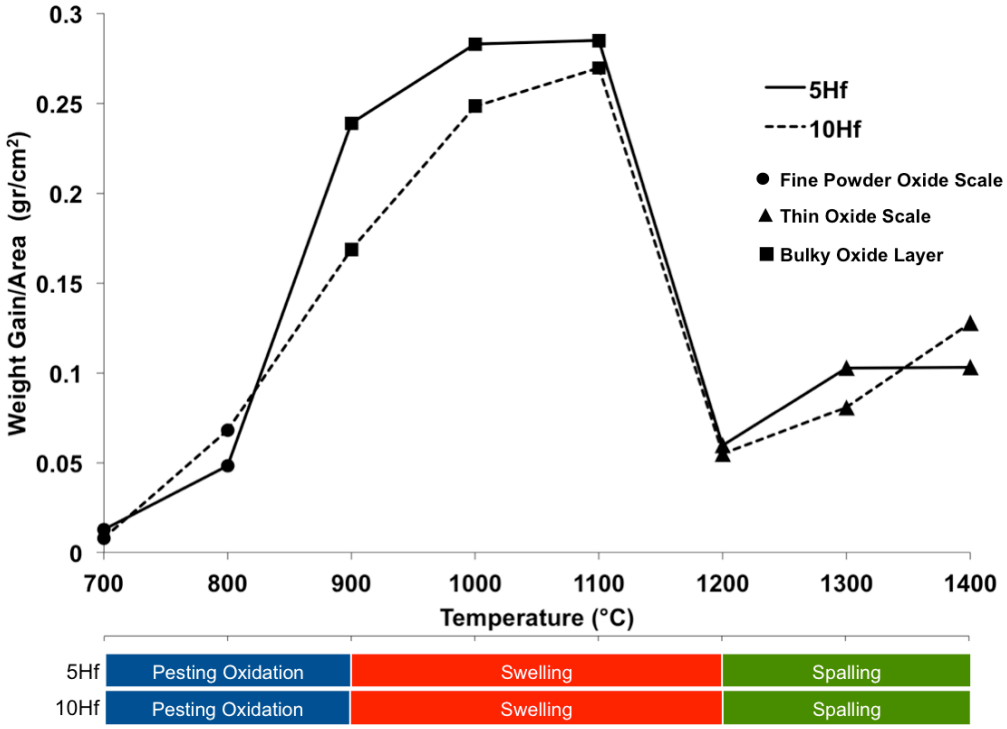

Figure 4.6. Isothermal oxidation curves for Nb-Cr-Si-5Hf and Nb-Cr-Si-10Hf alloys from 700 to 1400°C after 24 hours of exposure.

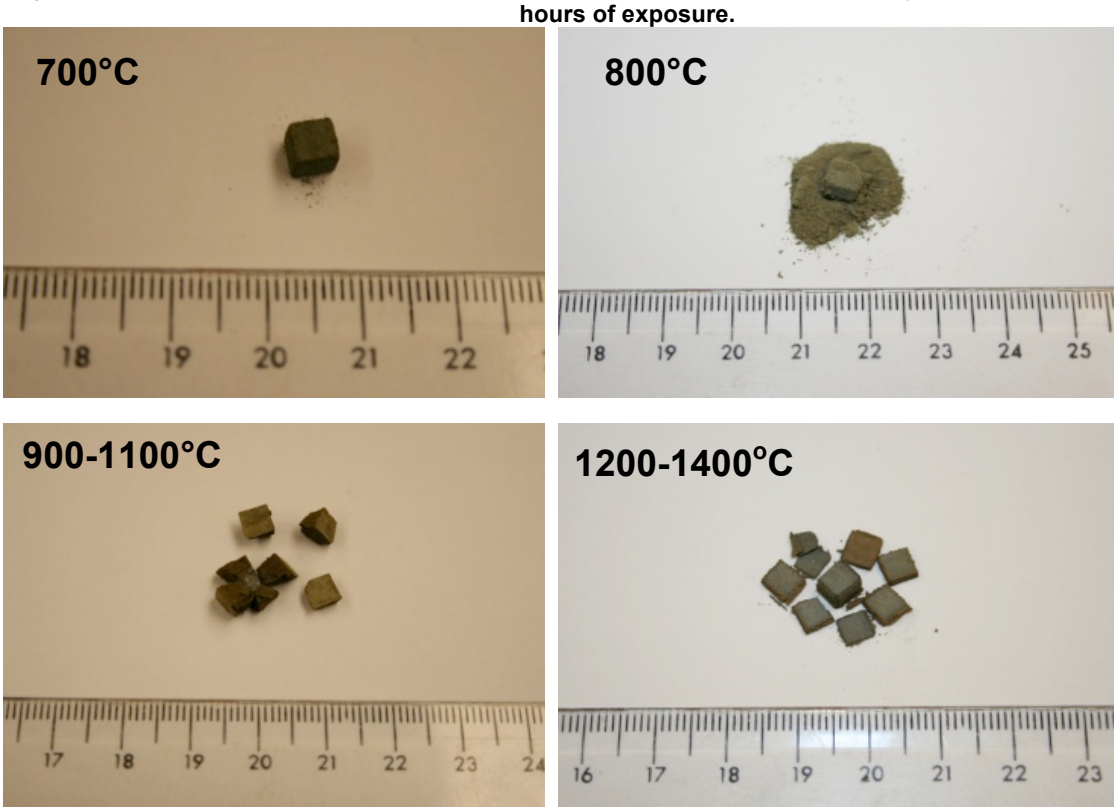

Figure 4.7. Oxidation products obtained from 5Hf alloy after isothermal oxidation for 24 hours. The oxidized products for isothermal oxidation test for 10Hf alloy were similar to those for 5Hf.

The first stage occurs at low temperature regime from 700-800^{o}C with best oxidation response based on their weight gain per unit area. At 700°C both samples exhibited little and very fine oxide particles. With an increase in the weight gain at 800°C the samples developed extensive formation of fine powder on the oxide product. The alloy with 10Hf addition is more prone to oxidation at 800°C with higher powder formation along with an increase in the weight gain. This temperature stage is characterized by the formation of powder indicating partial pesting behavior.

The second stage occurred at intermediate temperatures (900-1100^{o}C) in which a different oxidation behavior was observed with an increase in the weight gain. Oxidized samples at 900°C to 1100°C were converted to a complete bulky oxide except for the 5Hf alloy which shows partial oxide/metal interface in the center surrounded by the bulky oxide. It is important to note that in spite the high weight gain that the alloy with 5Hf addition showed at 900^{o}C, it has shown an oxide/metal interface compared to the 10Hf alloy that oxidized completely. Thus experiments of the oxidation kinetics at 900^{o}C shows that the Nb-Si-Cr system with lower Hf concentration is less susceptible to oxidation than those with higher concentration.

The final stage arose at higher temperatures above 1200°C with a decrease in the weight gain and where spallation of oxides scales occurred. This behavior can be attributed to the mismatch in the coefficients of thermal expansion (CTE) of the oxidation products creating stresses between the scale and the alloy that cause cracks and subsequent spallation of the oxide scales. For instance, the volume expansion caused by the formation of Nb_2O_5 and Cr_2O_3, is 107% and 169% of volume expansion respectively, produce large residual stresses that cause the breakdown and spallation of the scale [49].

4.3.2 Microstructure

The microstructures of the samples exposed to isothermal conditions are presented in Figures 4.8 and 4.9 for 5Hf and 10Hf alloy respectively. The microstructure shows excellent thermal stability since the alloys did not undergo phase transformation. Below 900°C the 5Hf alloy and below 800°C the 10Hf alloy showed similar microstructure as in the as-cast condition. However, when the samples were exposed to 1200°C hafnia started to appear preferentially inside the α and Laves phase, and within the interface between 5-3 silicide, Laves, and α phases. The morphology of hafnia changed through the sample from needle-like to bulky ones as shown in Figure 4.10. Backscatter electron (BSE) images show the microstructure formed at 1400°C for both alloys in Figure 4.11. Compared to the microstructure formed at 1200°C there was a significant increase in the volume fraction of hafnia inside the Laves and at the interfaces at 1400°C. Moreover, it was observed that the Hf rich areas were not present at temperatures above 1200°C suggesting that HfO_2 formed from the rich Hf areas in Nb_5Si_3 and Laves phases. This is consistent with previous studies that suggest the formation of hafnia from prior Hf rich areas of Nb_5Si_3 [3,4].

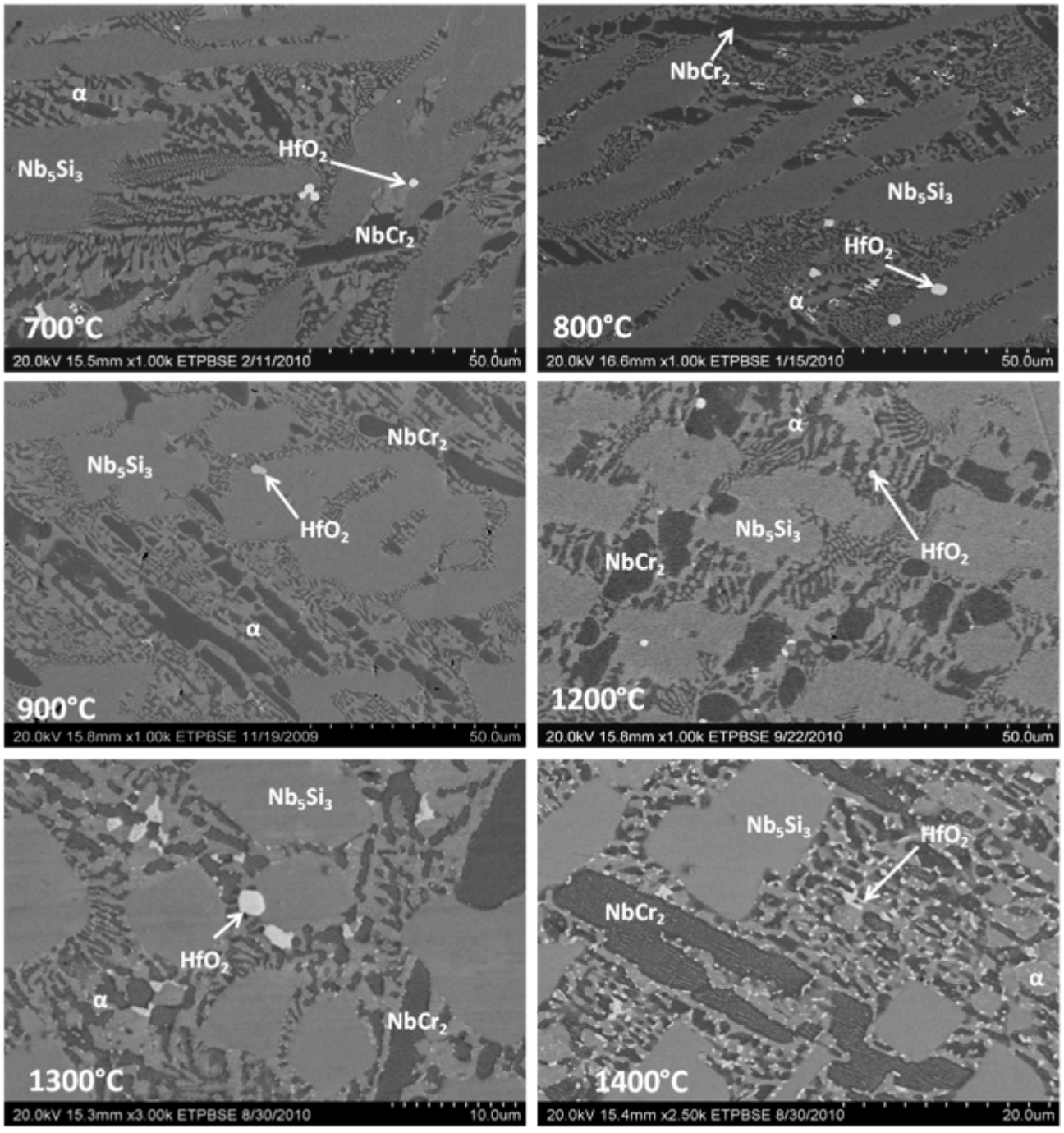

Figure 4.8. Microstructure of Nb-20Cr-20Si-5Hf alloy at 700°C-900°C, and 1200°C-1400°C.

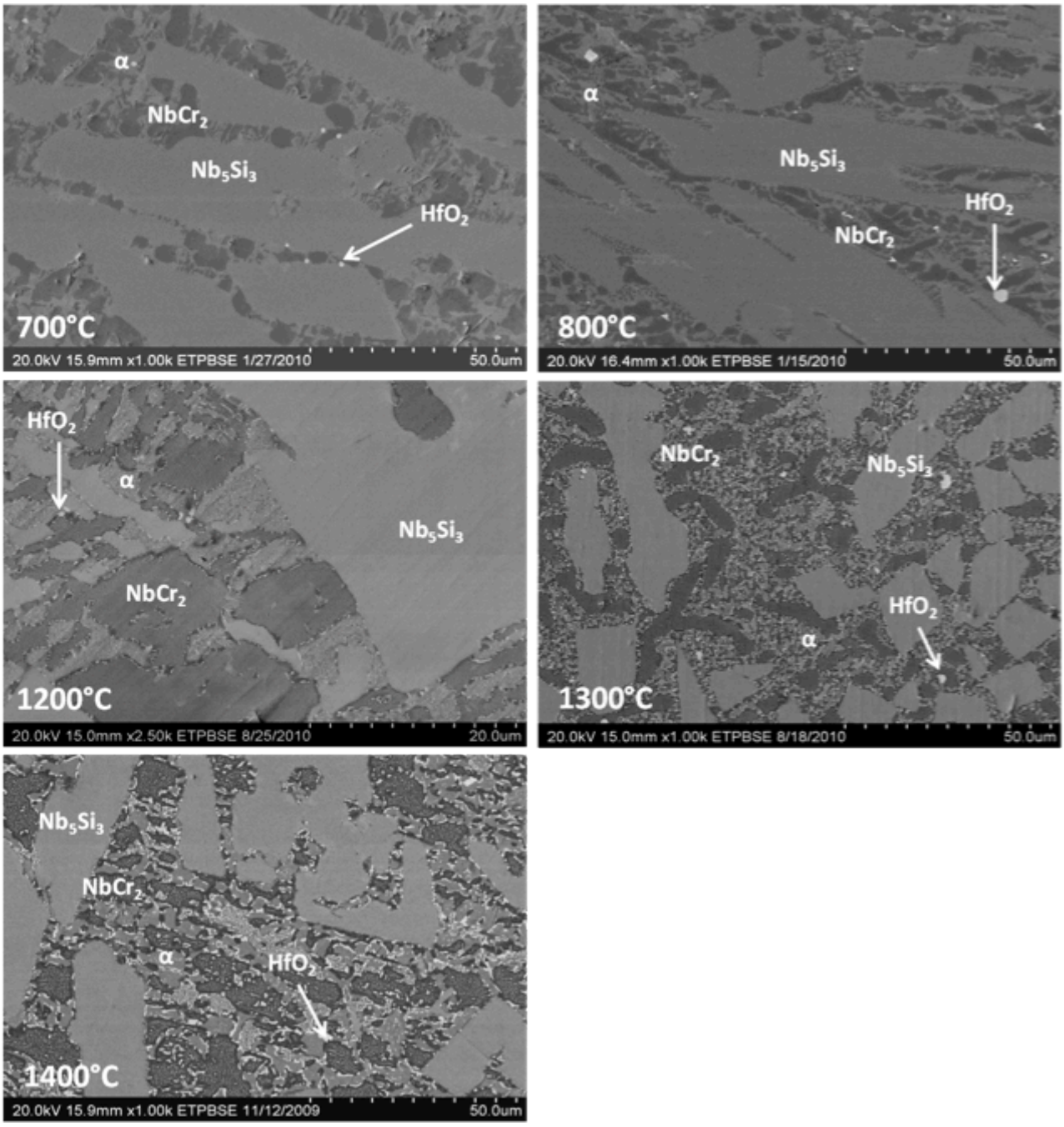

Figure 4.9. Microstructure of Nb-20Cr-20Si-10Hf alloy at 700°C-800°C, and 1200°C-1400°C.

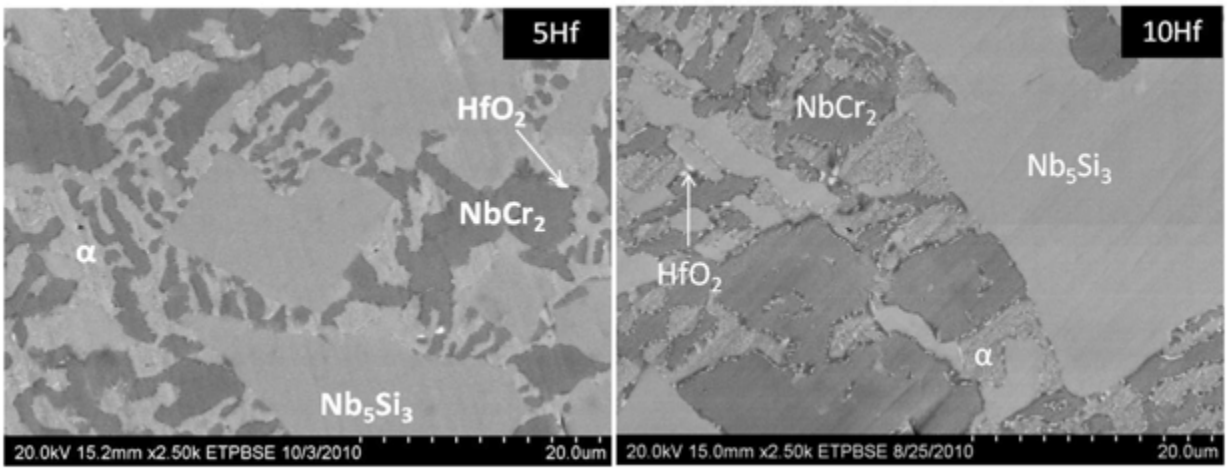

Figure 4.10. The microstructure developed in 5Hf and 10Hf alloy at 1200°C after STO.

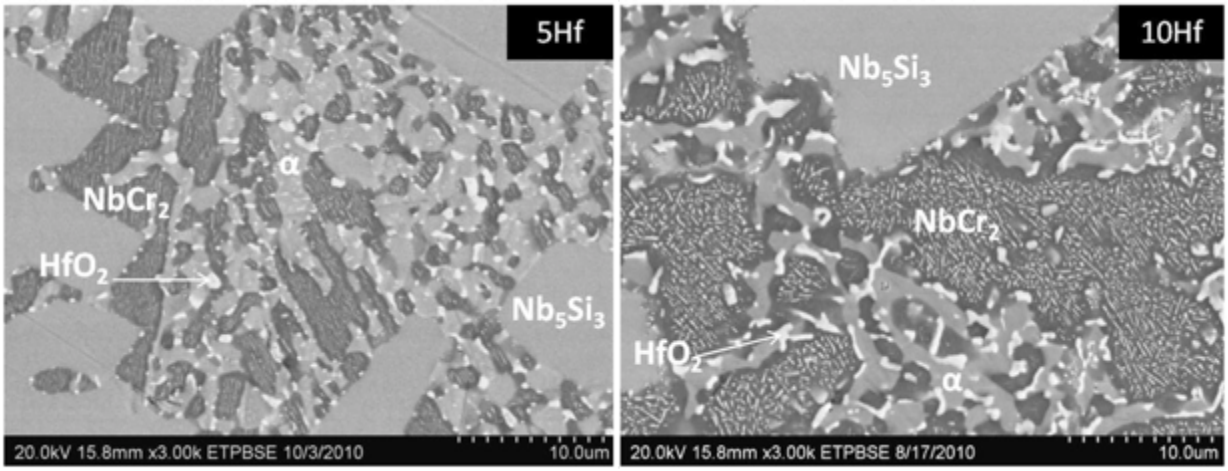

Figure 4.11. The microstructure developed in 5Hf and 10Hf alloy at 1400°C after STO.

4.3.3 Scanning Electron Microscopy Analysis of Oxide/Metal Interfaces

Figures 4.12 and 4.13 depict the BSE images of the composition and morphology of the oxide-metal interfaces as a function of temperature and alloy composition. The oxide scale formed at 700^{o}C and 800^{o}C appears extremely rough and discontinuous, probably caused by formation of oxides in the form of fine powder that avoided the formation of a continues scale. It appears that the major oxide is based on Nb_2O_5 (light gray) along with $CrNbO_4$ (dark gray) and some hafnium oxides (white phases). The

oxide layer developed at 900°C for 5Hf alloy shows better adherence to the substrate compared to those developed at lower temperatures. However, cracking parallel to the interface is visible. The oxide scale shows different oxides, Nb_2O_5, $CrNbO_4$, and HfO_2, as well as some patches of un-reacted $NbCr_2$ phase.

The oxide surfaces formed during exposure at 1300°C showed different morphology depending on the hafnium content. The oxide layer formed at 1300°C on the alloy with higher hafnium concentration appears relatively even, compared to the other alloy with lower Hf additions indicating that the addition of 5Hf to the alloy was detrimental creating an irregular oxide layer. Though, the 10Hf alloy shows a huge amount of porosity at the top surface. The dark gray phase was a mixture of Nb_2O_5 and SiO_2, while lighter areas were found to be $CrNbO_4$ with some oxide precipitates of HfO_2 distributed through the oxide scale.

A qualitative comparison between the alloy with 5Hf and 10Hf additions exposed at 1400°C are shown in Figure 4.14. Some porosity and cracking have been observed in the scale for both alloys. It appears that the main oxide is based on the ratio of Nb_2O_5 as gray phases and portions of un-reacted intermetallic $NbCr_2$ phase. It is important to spot portions of un-reacted 5-3 silicide phase at the oxide-metal interface for the 10Hf alloy. Composition analysis by EDS shows that the amounts of hafnium present in the Nb_5Si_3 phase for 10Hf alloy doubles the amount observed in the 5Hf alloy. The average amount of hafnium present at the 5-3silicide was 6.50at% for 5Hf alloy and 13.33at% for 10Hf alloy.

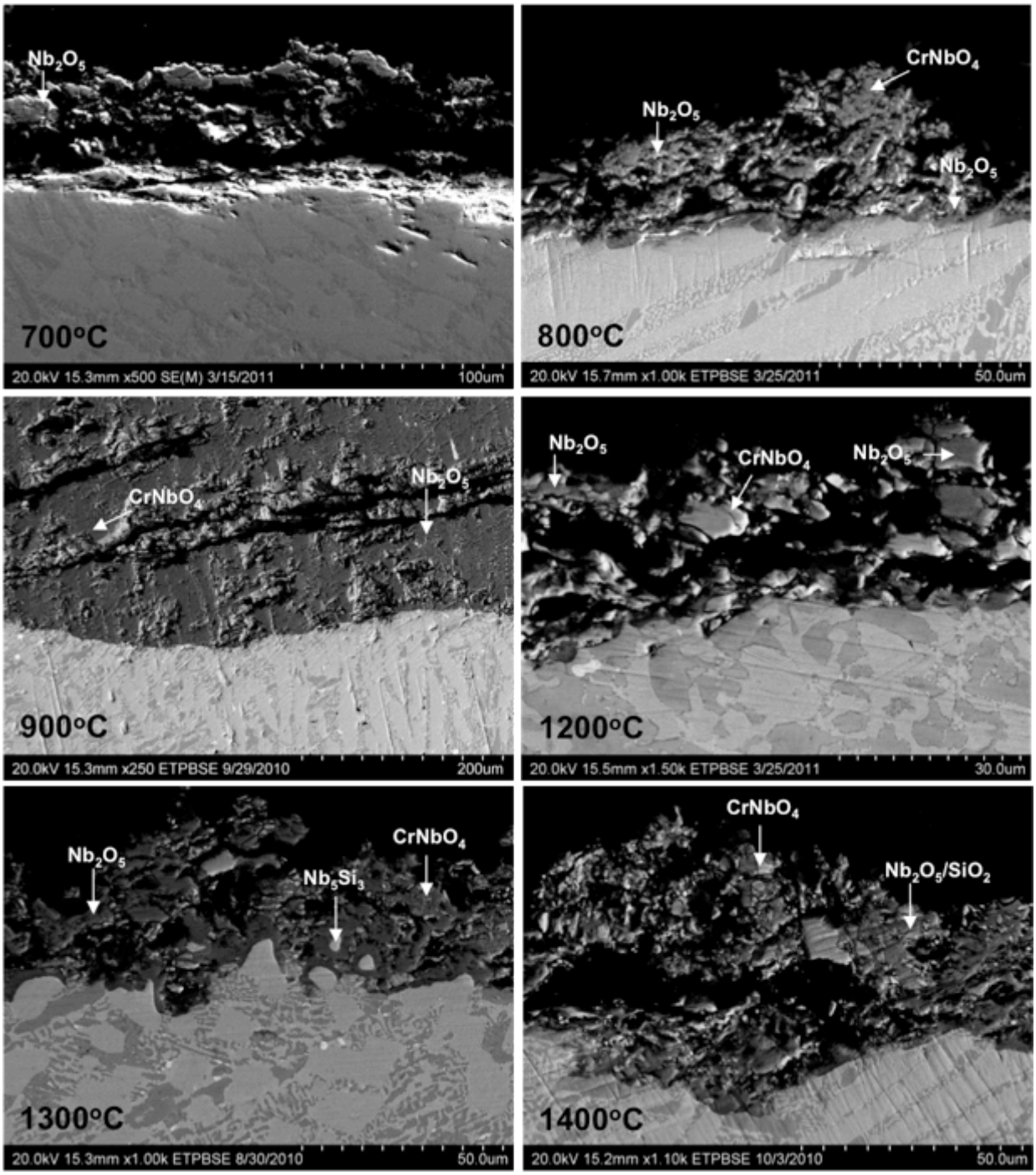

Figure 4.12. BSE images of the oxide-metal interfaces developed for 5Hf alloy under isothermal conditions.

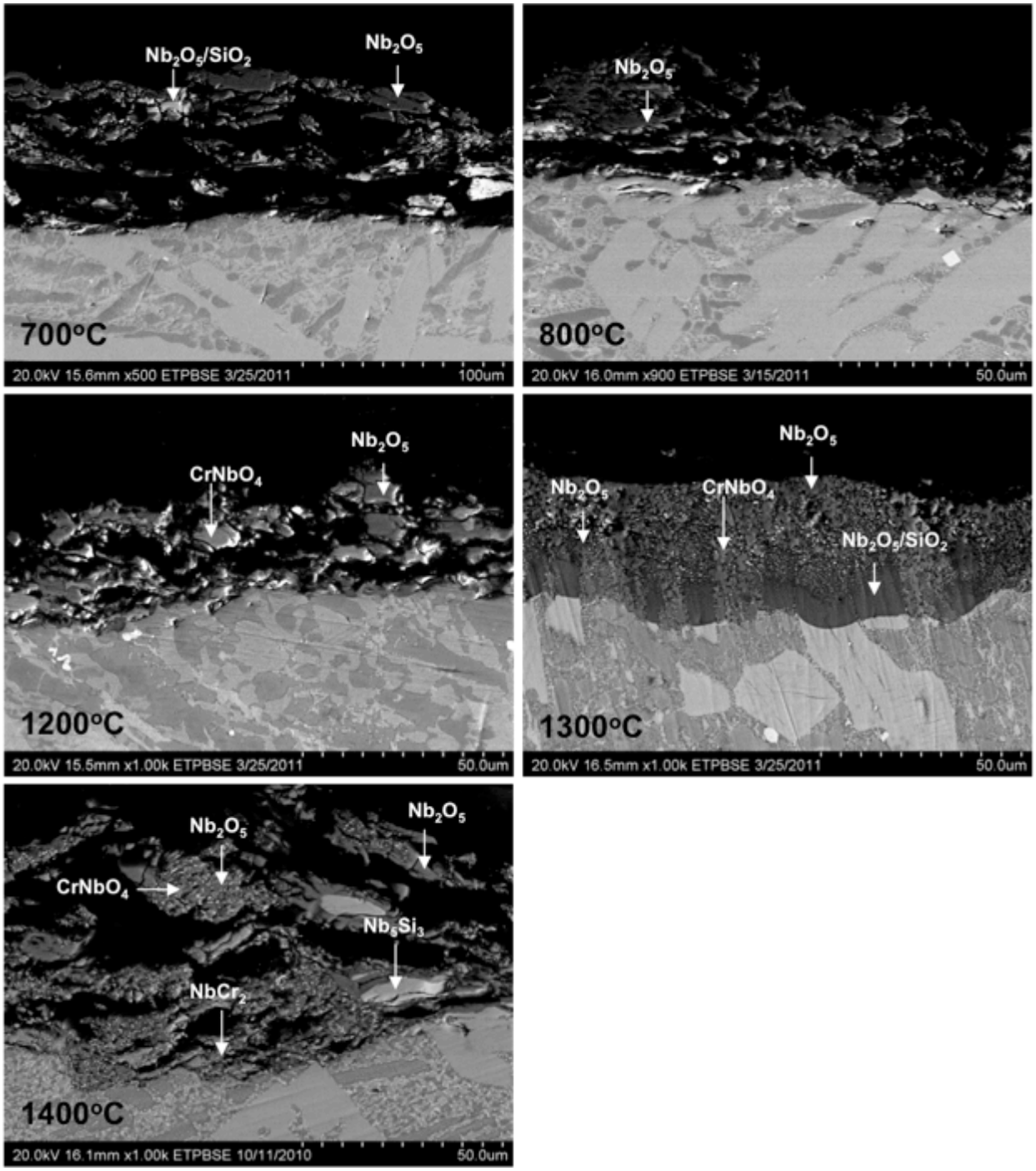

Figure 4.13. BSE images of the oxide-metal interfaces developed for 10Hf alloy under isothermal conditions.

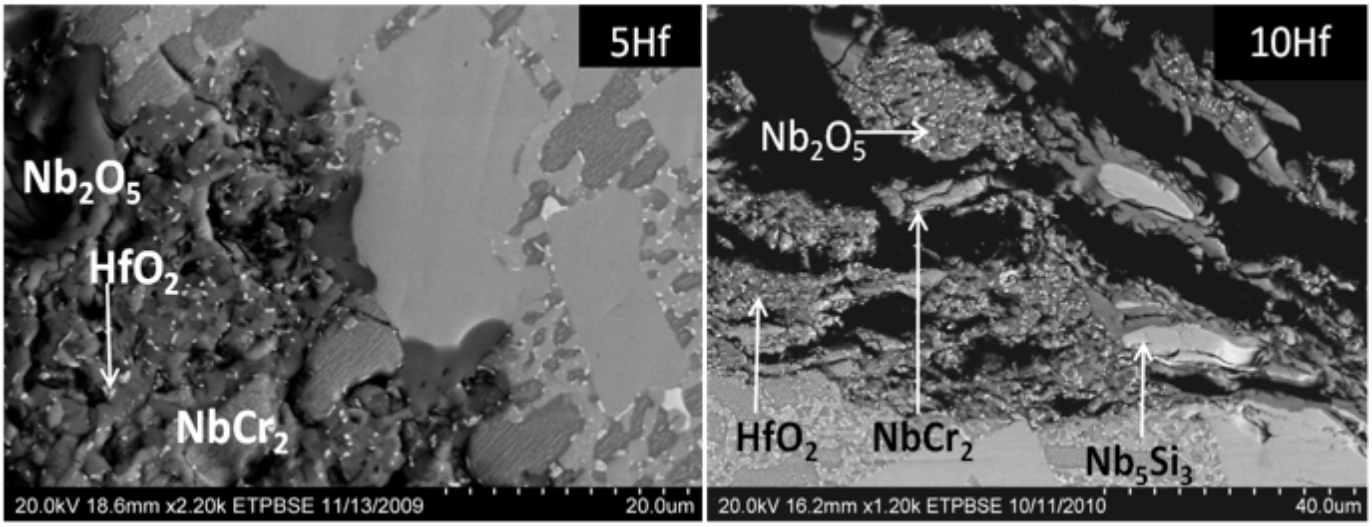

Figure 4.14. BSE images of the oxide-metal interfaces developed for 5Hf and 10Hf alloys exposed at 1400°C for 24 hours in static air.

Figure 4.15 shows the x-ray elemental analysis performed in the 10Hf alloy to observe the differences in the chemistry of the phases and oxides present at the oxide scale formed at 1400°C. Niobium and hafnium are almost uniformly distributed in the scale. While silicon is mostly concentrated at the un-reacted 5-3 silicide areas but no homogeneous oxide layer was observed. At this temperature regime spallation of oxide scales occurred. Analyses of both oxide scales formed at the solid surface were performed to further understand the oxidation resistance of both alloys at this temperature.

Figure 4.16 shows the scanning electron microscope (SEM) images of the morphology of the oxides formed on the metal surface at 1400°C for 5 and 10Hf alloys that appears to be related to the trends appearing in the kinetic data shown in Figure 4.6. It shows that scale formed on both alloys change with hafnium content. The alloy with 5Hf addition (with better oxidation resistance at 1400°C) have a more compact

oxide scale than 10Hf alloy that exhibits a porous oxide scale with limited ability to perform as a protective barrier.

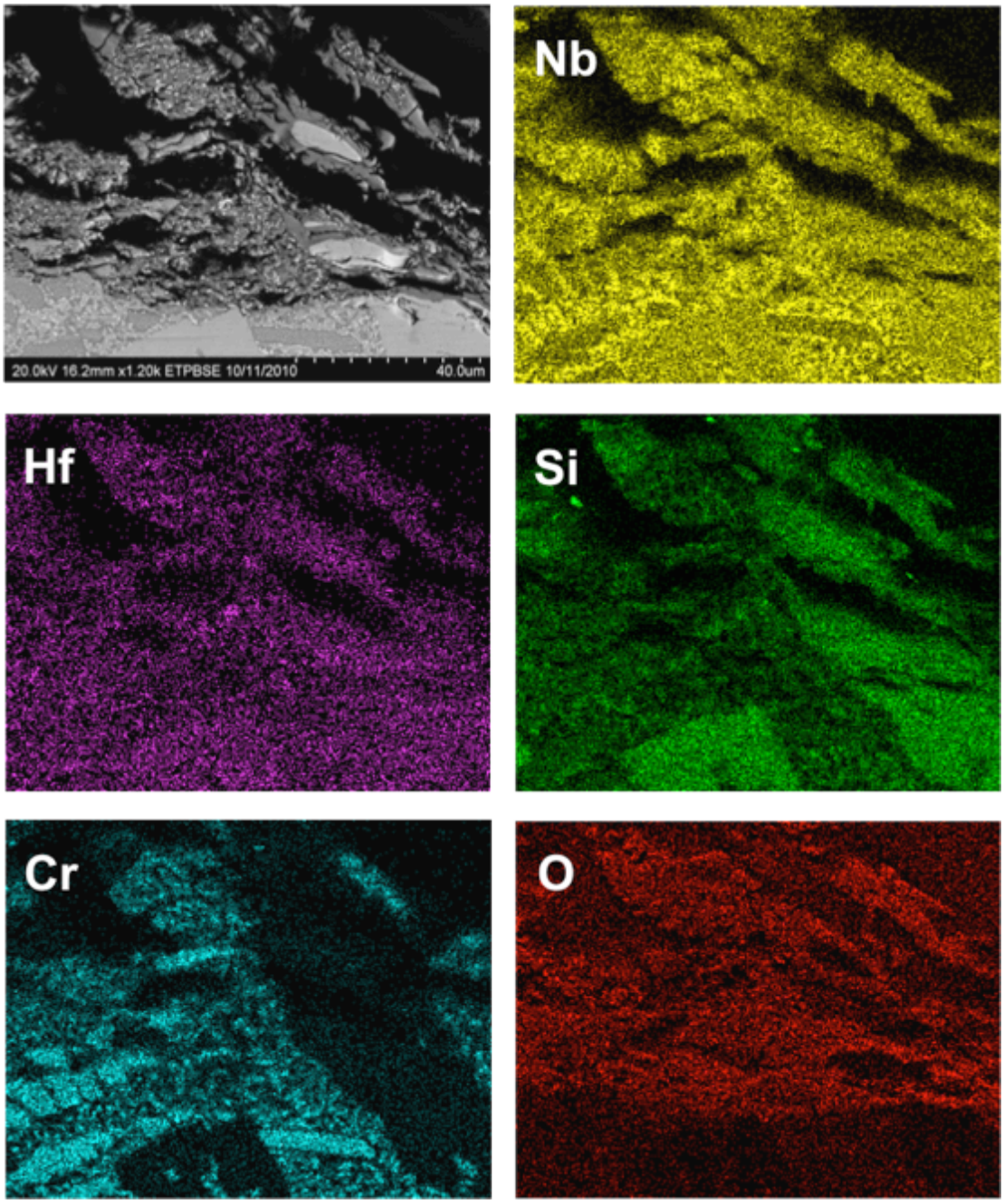

Figure 4.15. X-ray mapping on the oxide/metal interface of 10Hf alloy at 1400°C.

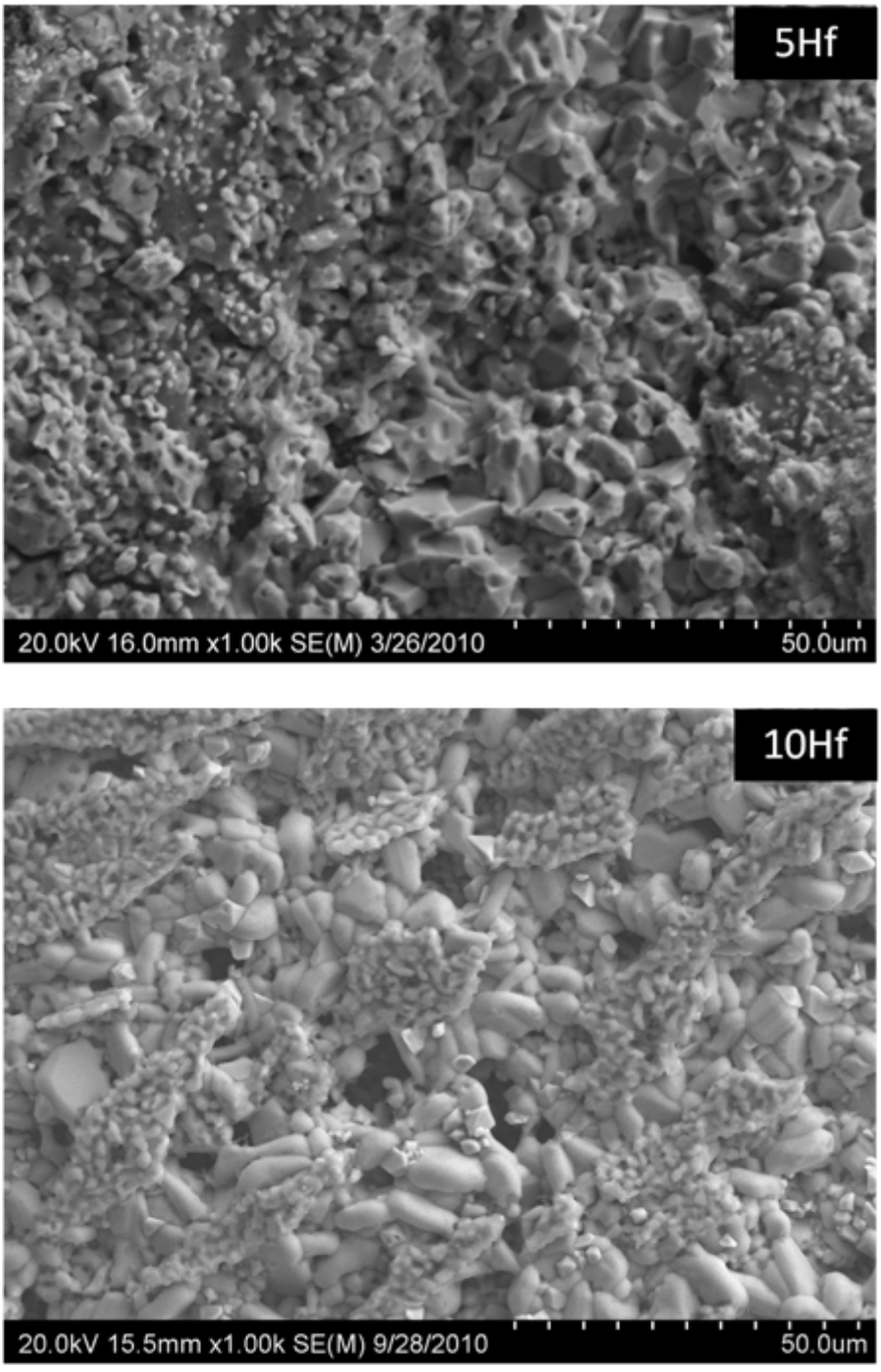

Figure 4.16. Scanning electron microscope (SEM) images of the morphology of the oxides formed on the metal surface at 1400°C for 5 and 10Hf alloys.

4.3.4 X-ray Diffraction Analysis of Oxidation Products

The oxides developed on the surface during oxidation were identified from X-ray diffraction, and the patterns obtained are shown in Figures 4.17 and 4.18. Also the combinations of the oxides present at each temperature found from the x-ray diffraction analyses are summarized in Table 4.1.The XRD technique detected Nb_2O_5, $CrNbO_4$ among other oxides. The predominant oxide formed at all temperatures was $CrNbO_4$. Three polymorphs of Nb_2O_5 were detected. Below 1000°C orthorhombic form of Nb_2O_5 was present, while the formation of monoclinic Nb_2O_5 initiated above 1100°C for 5Hf and 1200°C for 10Hf alloy. Experiments indicate that the intermediate temperature range where bulky oxide formed might be associated by the formation of base-centered monoclinic Nb_2O_5 since the lattice of Nb_2O_5 expands twice when it undergoes polymorphic changes from low temperature form (α-Nb_2O_5) to β-Nb_2O_5 [35]. The SiO_2 and HfO_2 formation has been limited to temperatures above 1300°C while hafnium silicate ($HfSiO_4$) was only present at the 10Hf alloy. $HfSiO_4$ oxide is a combination of HfO_2 and SiO_2 with a tetragonal structure.

Table 4.1. Summary of the combinations of the oxides for 5Hf and 10Hf alloys under isothermal experiments.

Temperature (°C)	o-Nb_2O_5	β-Nb_2O_5	m-Nb_2O_5	$CrNbO_4$	SiO_2	HfO_2	$HfSiO_4$
800	5Hf			5Hf			
900	5Hf			5Hf			
1000	5Hf	5Hf		5Hf			
1100		5Hf	5Hf	5Hf			
1200		5Hf	5Hf	5Hf			
1300			5Hf	5Hf	5Hf	5Hf	
1400			5Hf	5Hf	5Hf	5Hf	

5Hf 10Hf

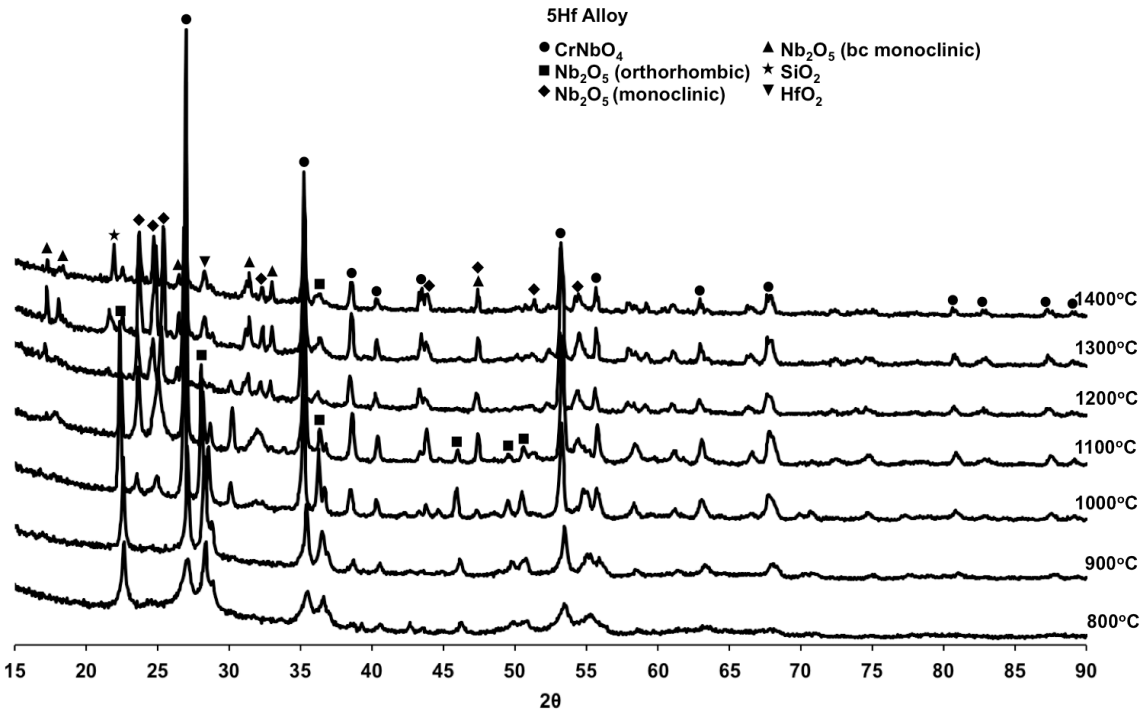

Figure 4.17. XRD pattern of the oxidation products obtained from 5Hf alloy under isothermal experiments.

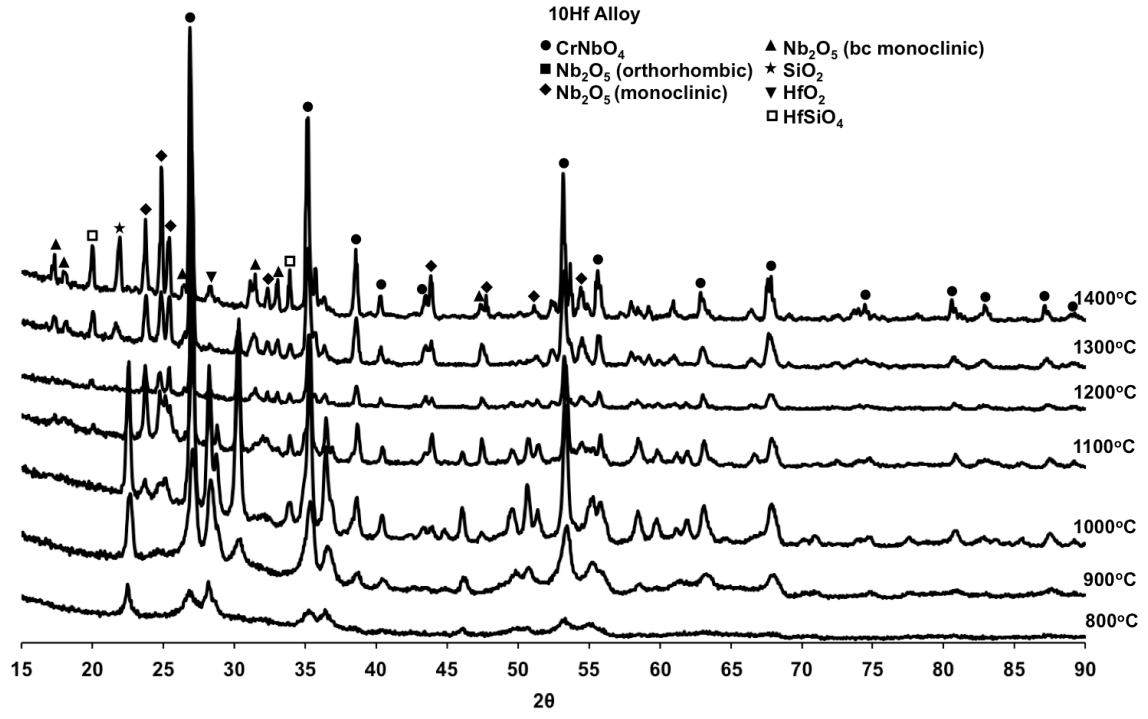

Figure 4.18. XRD pattern of the oxidation products obtained from 10Hf alloy under isothermal experiments.

4.4 Cyclic Oxidation

4.4.1 Oxidation Kinetics

The cyclic oxidation behavior of Nb-Si-Cr system with Hf additions has been investigated at different temperatures in terms of the variation in weight gain per unit area with time. Figures 4.19 and 4.20 show the plots for each alloy under cyclic conditions exposed at 700-800^{o}C and 1300^{o}C-1400^{o}C. In this study a complete oxide product was observed above 800°C for both alloys after 168hrs.

The oxidation behavior of 5Hf and 10Hf alloys follows parabolic and linear curves. On examination of the plots for the 5Hf alloy it is clear that the best oxidation resistance was obtained at 700^{o}C that shows lower weight gains and follows a linear behavior. On the contrary, the addition of 5Hf has been detrimental at 1400^{o}C showing a final weight after 168 hours of exposure to be approximately 6 times higher than that of the alloy exposed at 700^{o}C. Similar results were observed for 10Hf alloy showing linear oxidation curve at 700^{o}C. Nevertheless the alloy exposed at 1300^{o}C experienced a higher weight gain compared to the alloy exposed at 1400^{o}C. After 168 hours of exposure the samples exposed at 800^{o}C were converted completely into fine powder, whereas spallation of oxides scales occurred when the alloys were exposed in the high temperature regime (1300-1400^{o}C). The oxidation products observed at 700^{o}C were similar to the oxides formed at 800^{o}C along with thin oxide scales and an oxide-metal interface as shown in Figure 4.23.

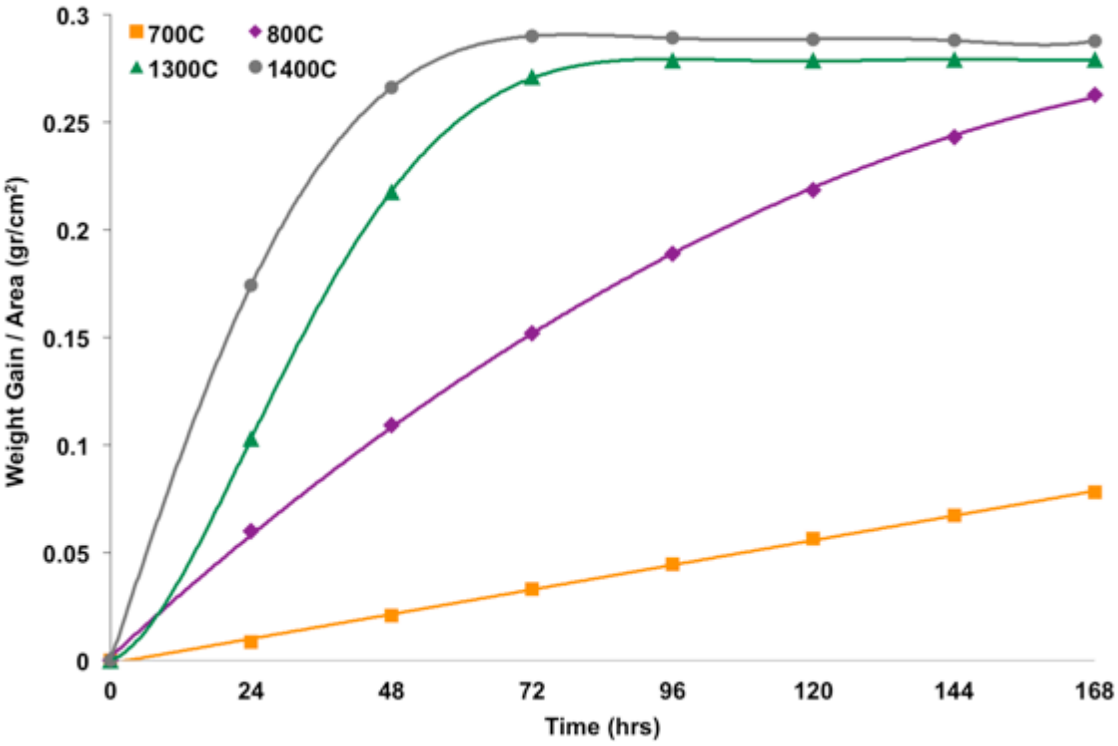

Figure 4.19. Cyclic oxidation curves for 5Hf alloy under cyclic conditions.

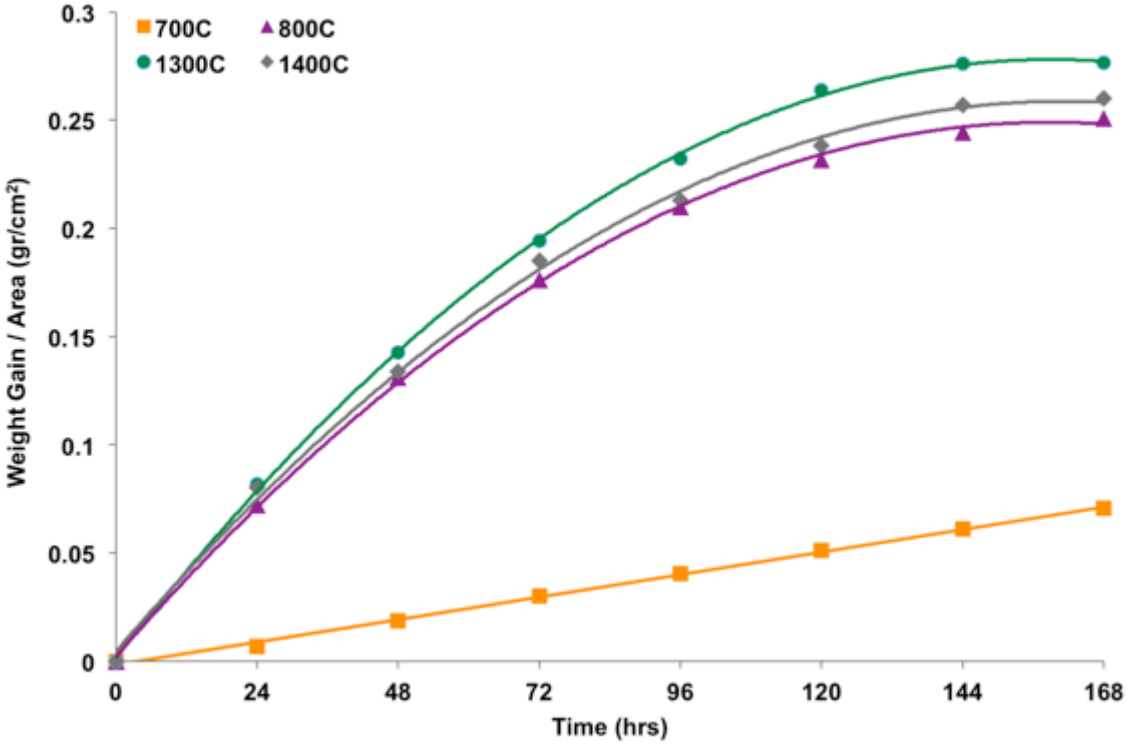

Figure 4.20. Cyclic oxidation curves for 10Hf alloy under cyclic conditions.

The cyclic oxidation curves for both alloys at 700°C and 800°C are presented in Figure 4.21. Cyclic oxidation experiments revealed that both alloys exhibit a good oxidation resistance at 700°C and 10Hf alloy shows lower weight gain per unit surface area. However, better oxidation resistance was observed for 5Hf after 168 hours of exposure at 800°C based on their weight gain per unit area. Alloy with 5Hf addition at 1300°C and 1400°C revealed a rapid oxidation rate during the first 48 hours of exposure to air followed by the stabilization of the weight gain per unit area for the subsequent five cycles.

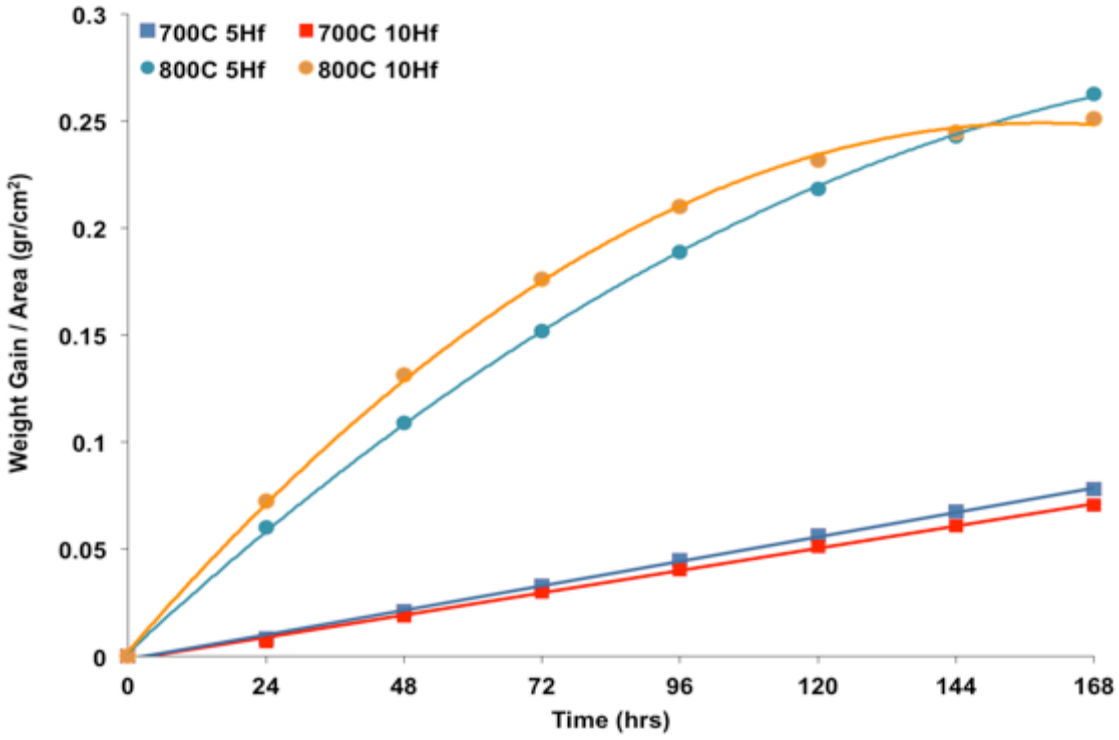

Figure 4.21. Cyclic oxidation curves for 5Hf and 10Hf alloys under cyclic conditions at 700-800°C.

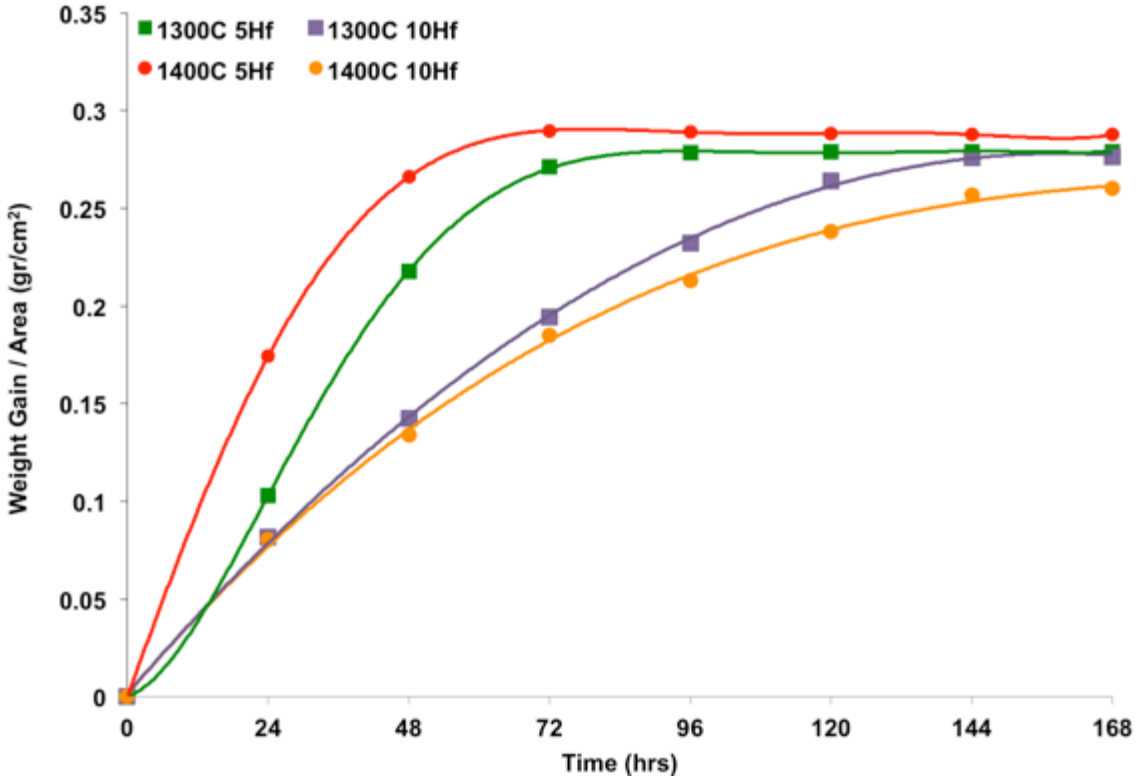

Figure 4.22. Cyclic oxidation curves for 5Hf and 10Hf alloys under cyclic conditions at 1300-1400°C.

4.4.2 Scanning Electron Microscopy Analysis of Oxide/Metal Interface

As mentioned all alloys investigated under cyclic conditions above 800°C after 168 hours were completely converted into oxides except for alloys exposed at 700°C. The oxidation product when the alloys were subjected to cyclic oxidation at 700°C suffered some powder formation as well as the formation of really thin oxide scales. Figure 4.23 shows the morphology of the oxidation products obtained for 5Hf alloy exposed at 700°C after 168 hours. The alloys followed a linear oxidation curve, which is expected due to the spallation of the oxide scales during cooling of the samples that allowed further oxidation and thus higher weight gains.

The metal/oxide interfaces that developed for 5Hf and 10Hf alloys are shown in Figure 4.24. The alloys present numerous cracks parallel to the substrate and porosity

at the interface between the metal and the oxide scale. The oxides formed during LTO were identified using XRD technique, EDS and BSE analysis. The oxides present at the scale were identified as Nb_2O_5 (dark gray), HfO_2 (white), and intermetallics that corresponded to un-reacted $NbCr_2$ phase. At 700^{o}C no protective oxide layer was formed, however the good oxidation resistance is attributed to the formation of several thin scales that protected the alloy at this temperature which spall possibly as a result by the stresses created upon cooling due to the differences in the coefficients of thermal expansion between the oxides formed. Moreover, metal/oxide interfaces were observed for the samples with 10Hf addition up to 72 hours while most of the Nb-based alloys with 5Hf addition oxidized completely after 48 hours.

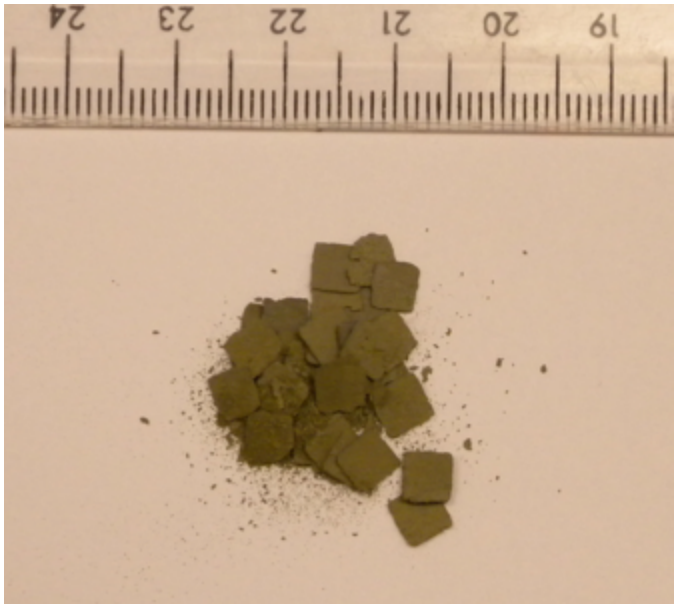

Figure 4.23. Oxidation products obtained for 5Hf alloy exposed at 700^{o}C after 168 hours.

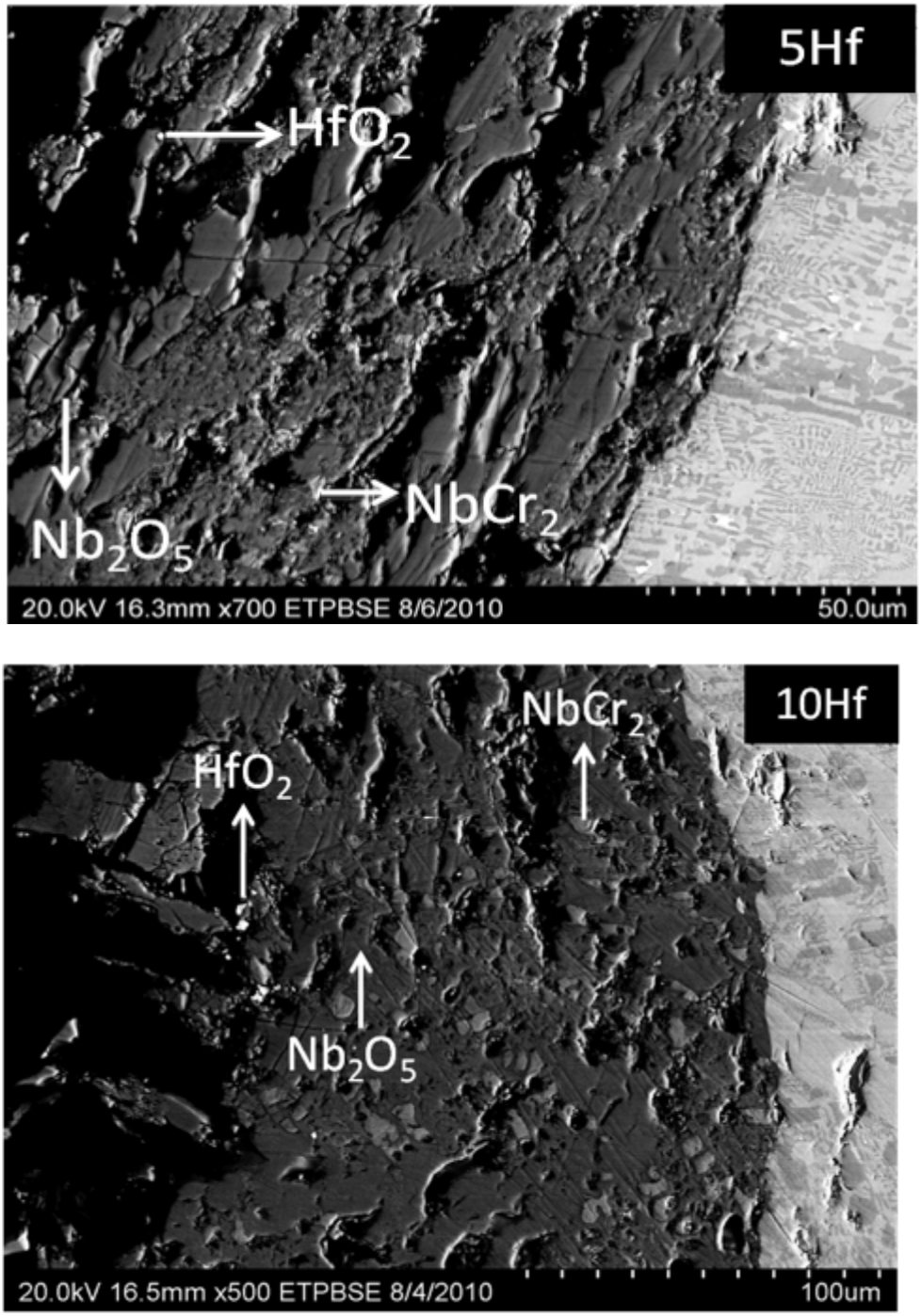

Figure 4.24. Metal/oxide interface for 5Hf and 10Hf alloys exposed at 700^{o}C after 168 hours.

4.4.3 X-ray Diffraction Analysis of Oxidation Products

The structure of the oxides formed on the surface during cyclic oxidation was deduced from X-ray diffraction in this study; diffraction peaks from these patterns are presented in Figures 4.25 and 4.26 in which polymorphic changes of Nb_2O_5 oxide were observed. Below 800°C the oxides were composed of low temperature modification of (orthorhombic) Nb_2O_5 as well as $CrNbO_4$. At higher temperatures the main oxides present were the monoclinic form of Nb_2O_5 and $CrNbO_4$. $HfSiO_4$ was detected only at 1300°C for 5Hf alloy and at 1400°C for 10Hf alloys. However, the formation of silicon oxide (cristobalite) was observed above 1300°C and hafnia only at 1400°C. The combinations of the oxides present at each temperature was deduce from the x-ray diffraction analyses are summarized in Table 4.2.

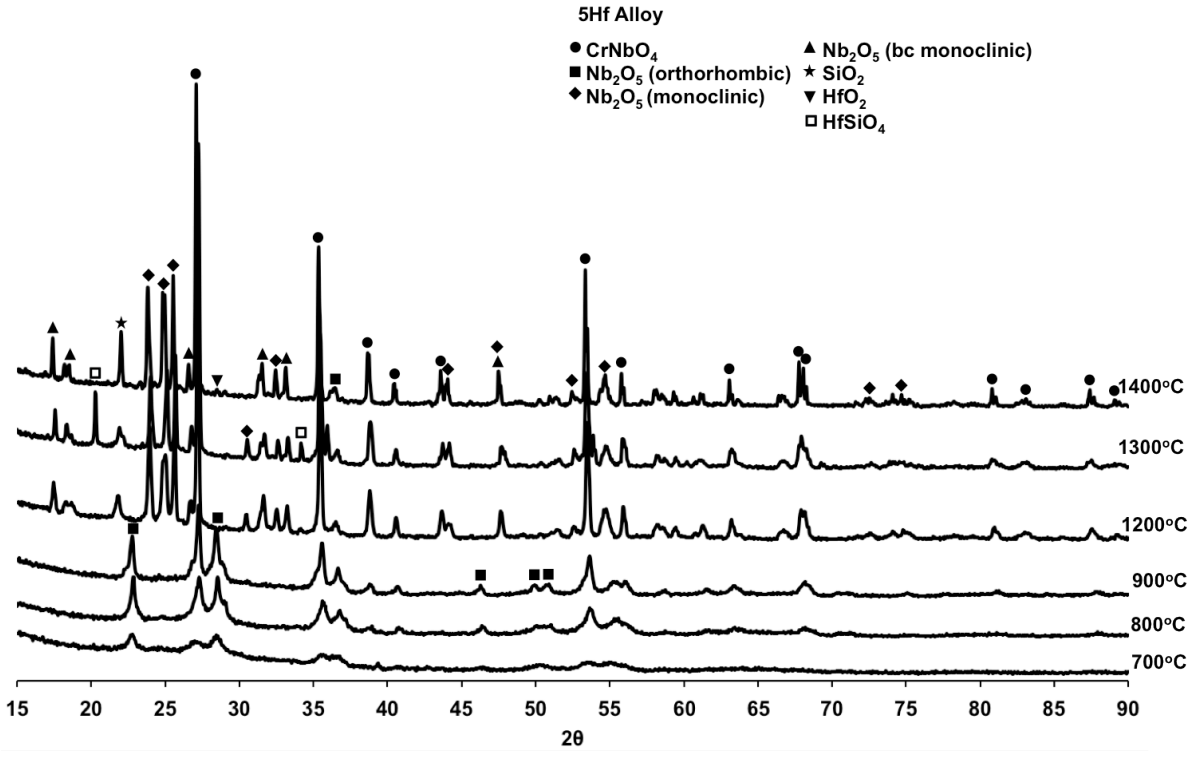

Figure 4.25. XRD pattern of the oxidation products obtained from 5Hf alloy under cyclic experiments.

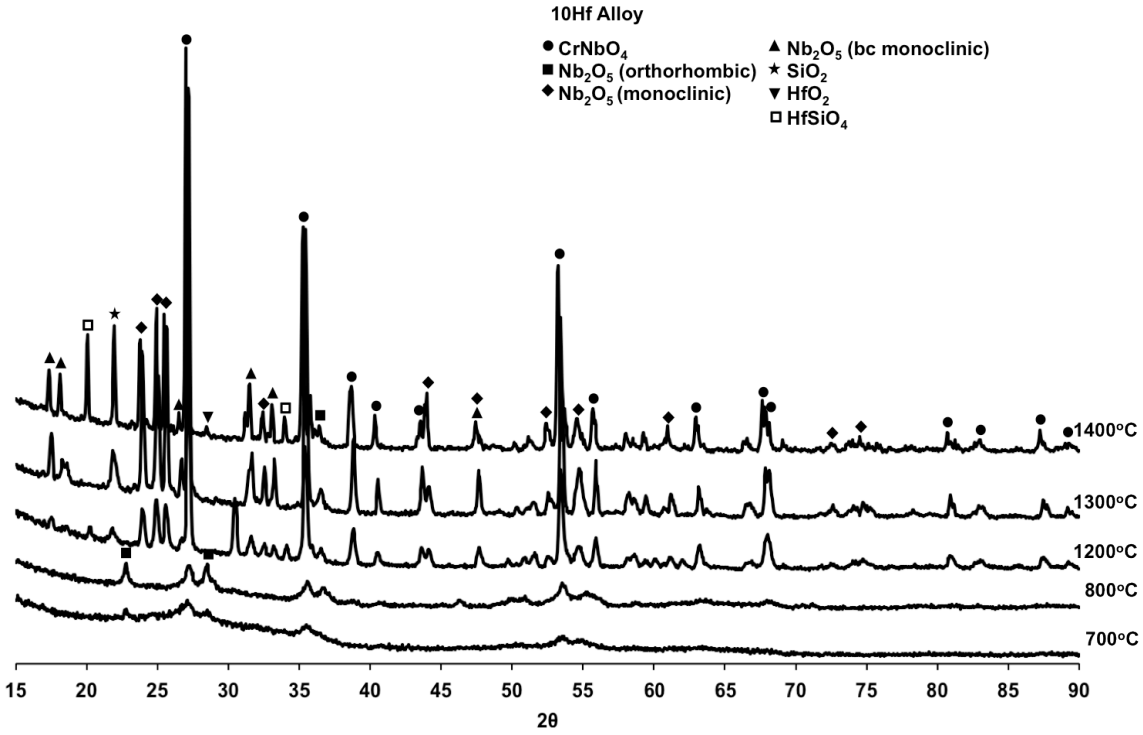

Figure 4.26. XRD pattern of the oxidation products obtained from 10Hf alloy under cyclic experiments.

Table 4.2. Summary of the combinations of the oxides for 5Hf and 10Hf alloys under cyclic experiments.

Temperature (°C)	o-Nb_2O_5	β-Nb_2O_5	m-Nb_2O_5	$CrNbO_4$	SiO_2	HfO_2	$HfSiO_4$
700	5Hf			5Hf			
800	5Hf			5Hf			
1300			5Hf	5Hf	5Hf		5Hf
1400			5Hf	5Hf	5Hf	5Hf	10Hf

5Hf 10Hf

4.5 Summary and Discussion of Results

The Nb-20Si-20Cr-5Hf and Nb-20Si-20Cr-10Hf alloys have been studied under isothermal and cyclic oxidation conditions in the temperature range of 700-1400^{o}C.

Quaternary isothermal sections calculated by Pandat^{TM} compute the presence of three stable phases for 5Hf alloy and four stable phases for 10Hf alloy. However, the as-cast microstructure for both alloys differs from the equilibrium phases calculated by the software. The as-cast microstructures of the alloys consisted of primarily four phases, Nb_{ss}, $NbCr_2$, Nb_5Si_3, and HfO_2. This inconsistency may be attributed to the non-equilibrium processing especially during casting of the alloys. XRD analysis confirmed the presence of three phases with their crystal structures; Nb_{ss} (BCC), $NbCr_2$ (C-14), and Nb_5Si_3 phase was present in the alpha and beta forms. The presence of high temperature form of Laves phase (C-14) can be stabilized by silicon at lower temperatures.

Microstructure of the alloys exposed for 24 hours show good phase stability with no phase transformations. At temperatures below 900^{o}C for 5Hf alloy and 800^{o}C for 10Hf alloy contain Nb_5Si_3, $NbCr_2$, Nb_{ss}, and hafnia microconstituents. In addition to the four phases, $NbCr_2$, and Nb_5Si_3 rich in hafnium were present. At higher temperatures an increase in hafnium oxide is observed. Hafnium being a reactive element can form HfO_2 by scavenging oxygen dissolved in other phases. It was observed that $NbCr_2$ and Nb_5Si_3 rich in hafnium were not present at temperatures higher than 1200^{o}C suggesting that the increase in volume fraction of HfO_2 developed from these hafnium rich phases. Also it was observed that partitioning of hafnia was preferentially located inside the Laves phases, as well as in the Nb_{ss} phase and at the interfaces between Nb_5Si_3,

$NbCr_2$, and Nb_{ss}. This is in agreement with previous studies where preferential formation of hafnia along the α/Nb_5Si_3 interfaces and inside α phase occurred [50].

Isothermal gravimetric studies at different temperatures have shown the susceptibility of the Nb-Si-Cr ternary system with Hf additions to be strongly dependent on the temperature. In the low temperature regime, both alloys show relatively low weight gain but have found the oxide scales with significant porosity and cracking along the metal oxide interface. The oxidation products obtained at 700 and 800^oC indicate partial pesting behavior. The explanation of this particular behavior has not been established yet, and further investigation is required. The combination of oxides present in both alloys was deduced from XRD, orthorhombic Nb_2O_5 and $CrNbO_4$. Improved oxidation behavior was observed at 700^oC with minimum weight gain per unit area from all temperatures studied in this work. At intermediate temperatures, the isothermal gravimetric studies have shown poor oxidation resistance regardless the different Hf additions to the Nb-Cr-Si system. The polymorphic change of based-centered monoclinic β-Nb_2O_5 from the low temperature form might be associated with the inadequate oxidation behavior observed at these temperatures that lead to the swelling of the metals since the lattice of Nb_2O_5 expands twice when it undergoes polymorphic changes from low temperature form (α-Nb2O5) to β- Nb_2O_5 [35].

The lower weight gain observed in the 10Hf alloy at 1300^oC can be attributed to the improved adherence of the oxide scale to the substrate that protected the alloy from further oxidation. Nonetheless, the alloys with higher concentration of hafnium have shown higher weight gain at 1400^oC. Possible explanation of this increase could be the rapid surface diffusion of oxygen through the porous scale formed at the metal surface affecting its oxidation behavior. The SiO_2 and HfO_2 were detected above 1300°C. The

enhance oxidation behavior can be attributed to the presence of SiO_2 and $CrNbO_4$ forming as protective oxides, and HfO_2 due to its high affinity for oxygen that prevent further oxygen diffusion to the metal. Moreover, the addition of 10 at.% hafnium appears to be important to enhance the oxidation resistance of the Nb_5Si_3 phase that did not oxidized selectively at 1400^{o}C. The detail of this specific behavior has not been really understood but it indicates that the Nb solid solution phase oxidized selectively, and the Nb_5Si_3 remained unaffected.

Cyclic oxidation experiments at different temperatures have revealed the vulnerability of the alloy system with hafnium additions to be dependent on the temperature and time. Impressive oxidation resistance was observed at 700^{o}C for both alloys indicating the beneficial effect of the presence of hafnium at this temperature. The oxide/metal interface contained severe cracking with the presence of orthorhombic Nb_2O_5, $CrNbO_4$, hafnia, and $NbCr_2$ phase. The improved oxidation resistance at this temperature can be attributed to the addition of hafnium that changed the oxidation products observed under isothermal conditions. The oxide morphology obtained under static oxidation experiments was fine powder, however, under cyclic condition the oxide products were thin oxide scales that possibly protected the alloy form further oxidation. After exposure at 800^{o}C the samples were converted completely into powder and consisted of orthorhombic Nb_2O_5 and $CrNbO_4$. At higher temperatures (1300-1400^{o}C) the alloys show poor oxidation behavior by oxidizing completely. Oxidation products observed at these temperatures were the high temperature forms of Nb_2O_5, $CrNbO_4$, HfO_2, SiO_2, and $HfSiO_2$. The beneficial effect of hafnium under cyclic oxidation was observed for the 10Hf alloy where fragments of metal remain unaffected up to 72 hours while the alloys with 5 at.% Hf additions oxidized completely after 68 hours of exposure.

CHAPTER 5

CONCLUSIONS

The effect of small additions of hafnium on the oxidation kinetics was evaluated.

1. As-cast microstructures for Nb-20Si-20Cr-(5,10)Hf alloys consist of four phases: solid solution (α), $NbCr_2$, Nb_5Si_3, and HfO_2. The as-cast microstructure for both alloys differs from the equilibrium phases calculated by PANDATTM software.
2. Alloys showed good thermal stability and remain as a four-phase alloy at all temperatures.
3. Selective internal oxidation of hafnium occurred at temperatures above 1200^{o}C due to the high thermodynamic stability of hafnia.
4. Isothermal and cyclic gravimetric studies have shown the susceptibility of the alloys to be strongly dependent on temperature and time.
5. Alloys reveal different morphology of the oxide products under isothermal experiments. At the low temperature regime (700-800^{o}C), powder was the final oxide product, swollen oxides at the intermediate range (900-1100^{o}C), and spallation of oxide scales at higher temperatures (1200-1400^{o}C).
6. Best oxidation resistance was observed at 700^{o}C for both alloys with lower weight gain under isothermal and cyclic conditions.
7. Partial pesting occurred when the samples were exposed to 700 and 800°C after 24 hours of exposure. This behavior is not completely understood and steps need to be taken to mitigate this problem.
8. Nb-20Cr-20Si-10Hf alloy exhibits better oxidation resistance compared to Nb-20Cr-20Si-5Hf alloy at 700°C, 1200°C and 1300°C based on the weight gain per unit area.

9. Formation of base-centered monoclinic form (β- Nb_2O_5) could be responsible for the formation of bulky oxide at intermediate temperatures.
10. Cyclic oxidation investigations indicate that the addition of hafnium was detrimental at temperatures above 800^{o}C.

REFERENCES

[1] B.P. Bewlay, M.R. Jackson, J.C. Zhao, P.R. Subramanian, M.G. Mendiratta, and J.J. Lewandowski. “Ultrahigh-temperature Nb-silicide-based composites.” *MRS Bulletin*, Septermber 2003, 646-653.

[2] B.P. Bewlay, M.R. Jackson, J.C. Zhao, and P.R. Subramanian. “A review of very-high-temperature Nb-silicide-based composites.” *Metall. Mater. Trans. A.*, 2003, vol. 34A, 2043-2052.

[3] J. Geng, and P. Tsakiropoulos. “A study of the microstructures and oxidation of Nb-Si-Cr-Al-Mo in situ composites alloyed with Ti, Hf, and Sn.” *Intermetallics*, 2007, vol. 15, 382-395.

[4] I. Grammenos, and P. Tsakiropoulos. “Study of the role of Al, Cr, and Ti additions in the microstructure of Nb-18Si-5Hf base alloys.” *Intermetallics*, 2010, vol. 18, 242-253.

[5] P.R. Subramanian, M.G. Mendiratta, and D.M. Dimiduk. “The development of Nb-based advanced intermetallic alloys for structural applications.” *Journal of Metals*, 1996, vol 48, 33-38.

[6] B.P. Bewlay, M.R. Jackson, and H.A. Lipsitt. “The balance of mechanical properties and environmental properties of a multielement Niobium-Niobium Silicide-based in situ composite.” *Metall. Mater. Trans. A.*, 1996, vol. 27A, 3801-3808.

[7] M.R. Jackson, B.P. Bewlay, R.G. Rowe, D.W. Skelly, and H.A. Lipsitt. “High-temperature refractory metal-intermetallic composites.” *Journal of Metals*, 1996, vol. 48, 39-44.

[8] K.S. Chan. “Cyclic oxidation response of multiphase Niobium-based alloys.” *Metall. Mater. Trans. A.*, 2004, vol. 35A, 589-597.

[9] J. Geng, P. Tsakiropoulos, and G. Shao. “Oxidation of Nb-Si-Cr-Al in situ composites with Mo, Ti, and Hf additions.” *Mater. Sci. Eng. A.*, 2006, vol. 441, 26-38.

[10] J. Geng, and P. Tsakiropoulos. “A study of the effects of Hf and Sn additions on the microstructure of Nb_{ss}/Nb_5Si_3 based in situ composites.” *Intermetallics*, 2007, vol. 15, 69-76.

[11] Y. Murayama, and S. Hanada. “High temperature strength, fracture toughness and oxidation resistance of Nb-Si-Al-Ti multiphase alloys.” *Science and Technology of Advanced Materials*, 2002, vol. 3, 145-156.

[12] Y. Saito, B. Onay, and T. Maruyama. “The reactive element effect (REE) in oxidation of alloys.” *Journal de Physique IV*, 1993, vol. 3, 217-230.

[13] B.A. Pint. “Experimental observations in support of the dynamic-segregation theory to explain the reactive-element effect.” *Oxidation of Metals*, 1996, vol. 45, 1-37.

[14] P.Y.Hou, and J. Stringer. “The effect of reactive element additions on the selective oxidation, growth and adhesion of chromia scales.” *Mater. Sci. Eng. A.*, 1995, vol. 202, 1-10.

[15] J. Stringer. “The reactive element effect in high temperature corrosion.” Mater*. Sci. Eng. A.*, 1989, vol. 120-121, 129-137.

[16] K.S. Chan. “Cyclic-oxidation resistance of niobium-base in situ composites: modeling and experimentation.” *Oxidation of Metals*, 2004, vol. 61, 165-194.

[17] S.A. Bradford. *Fundamentals of Corrosion in Gases*. ASM Metals Handbook, vol. 13. Materials Park, OH: ASM International, 9th edition, 1990.

[18] A.S Khanna. *Introduction to High Temperature Oxidation and Corrosion*. Materials Park, OH: ASM International, 2002.

[19] N. Birks, G.H. Meier, and F. Perttit. *Introduction to the High-Temperature Oxidation of Metals*. United Kingdom: Cambridge University Press, 2nd edition, 2006.

[20] D.A. Jones. *Principles and Prevention of Corrosion*. Upper Saddle River, NJ: Prentice Hall, Inc., 2nd edition, 1996.

[21] S.R.J Saunders, and J.R. Nicholls. *Oxidation, Hot Corrosion and Protection of Metallic Materials*. In: R.W. Cahn and P. Haasen Editors. North-Holland, Amsterdam: Elsevier sience. Physical Metallurgy 4th edition, 1983.

[22] D.P. Whittle, and J. Stringer. “Improvement in properties: additives in oxidation resistance.” *Phil. Trans. R. Soc. Lond. A.*, 1980, vol. 295, 309-329.

[23] D. Yi, D. Li, H. Liu, C. Wu, and H. Zhou. “Microstructure and oxidation behavior of mechanically alloyed Nb-based multiphase superalloy.” *Journal of Iron and Steel Research*, 2007, vol. 14, 1-6.

[24] T. Murakami, S. Sasaki, K. Ichikawa, and A. Kitahara. “Oxidation resistance of power compacts of the Nb-Si-Cr system and Nb3Si5Al2 matrix compacts prepared by spark plasma sintering.” *Intermetallics*, 2001, vol. 9, 629-635.

[25] K. Zelenitsas, and P. Tsakiropoulos. “Effect of Al, Cr, and Ta additions on the oxidation behavior of Nb-Ti-Si in situ composites at 800^{o}C.” *Mater. Sci. Eng. A*., 2006, vol. 416, 269-280.

[26] T. Murakami, S. Sasaki, K. Ichikawa, and A. Kitahara. “Microstructure, mechanical properties and oxidation behavior of Nb-Si-Al and Nb-Si-N powder compacts prepared by spark plasma sintering.” *Intermetallics*, 2001, vol. 9, 621-627.

[27] F. Zamoum, T. Benlaharche, N. David, R. Podor, and M. Vilasi. “Kinetics of high temperature oxidation of (Nb,Co,Cr)7Si6 and (Nb,Co,Cr)8Si7 silicide compounds.” *Intermetallics*, 2008, vol. 16, 498-507.

[28] M.P. Brady, J.H. Zhu, C.T. Liu, P.F. Tortorelli, and L.R. Walker. “Oxidation resistance and mechanical properties of Laves phase reinforced Cr in-situ composites.” *Intermetallics*, 2000, vol. 8, 1111-1118.

[29] C. Chen, C. Zhou, S. Gong, S. Li, Y. Zhang, and H. Xu. “Deposition of Cr-modified silicide coatings on Nb-Si system intermetallics. *Intermetallics*, 2007, vol. 15, 805-809.

[30] B.P Bewlay, M.R. Jackson, and P.R. Subramanian. “Processing high-temperature refractory-metal silicide in-situ composites.” *Journal of Metals*, vol. 41, 1999, 32-36.

[31] J.C. Zhao, M.R. Jackson, L.A. Peluso. “Determination of the Nb-Cr-Si phase diagram using diffusion multiples.” *Acta Materialia*, 2003, vol. 51, 6395-6405.

[32] S.Y. Qu, Y.F. Han, and Y.W. Kang. “Effects of Ti, Al and Hf on niobium silicides formation in the Nb-Si in situ composites.” *Science in China Series E: Tech. Sci.*, 2009, vol. 52, 37-40.

[33] F. Chu, D.J. Toma, P.G. Kotula, S. Gerstl, T.E. Mitchell, I.M. Anderson, and J. Bentley. “Phase stability and defect structure of the C15 laves phase $Nb(Cr,V)_2$.” *Acta Materialia*, 1998, vol. 46, 1759-1769.

[34] J. Geng, G. Shao, and P. Tsakiropoulos. “Study of three-phase equilibrium in the Nb-rich corner of Nb-Si-Cr system.” *Intermetallics*, 2006, vol. 14, 832-837.

[35] S.K. Varma, C. Parga, K. Amato, and J. Hernandez. “Microstructure and high temperature oxidation resistance of alloys from Nb-Cr-Si system.” *Journal of Material Science*, 2010, vol. 45, 3931-3937.

[36] B.P. Bewlay, Y. Yang, R.L. Casey, M.R. Jackson, and Y.A. Chang. “Effect of Cr addition on the phase equilibria of the Nb-Si system.” *Materials Research Society Symposium Proceedings*, 2007, vol. 980, 333-338.

[37] J.S. Sheasby and G.R. Wallwork. “The parabolic oxidation kinetics of niobium.” *Journal of the Electrochemical Society*, 1966, vol. 113, 1255-1257.

[38] J.S. Sheasby and W.W. Smeltzer. “Oxygen tracer studies of the oxidation of niobium.” *Oxidation of Metals*, 1981, vol. 15, 215-219.

[39] T. Hurlen. “Oxidation of niobium.” *Journal of the Institute of Metals*, 1960, vol. 89, 273-280.

[40] H. Schäfer, R. Gruehn, F. Schulte. “The modifications of niobium pentoxide.” *Angew. Chem. Int. Edit. Eng*., 1966, vol. 5, 40-52.

[41] M.P. Arbuzov and V.G. Chuprina. “The oxidation of niobium and the structure of niobium oxides.” *Izvestiya VUZ. Fizika*, 1965, No. 2, 129-133.

[42] H. Goldschmidt. “A high-temperature X-ray investigation of niobium pentoxide and some problems concerning the oxidation of Niobium.” *Journal of the Institute of Metals*, 1959, vol. 87, 235-239.

[43] D.Yao, C. Zhou, J. Yang, and H. Chen. “Experimental studies and modeling of the oxidation of multiphase niobium-base alloys.” *Corrosion Science*, 2009, vol. 51, 2619-2627.

[44] Y. Liu, M.J. Kramer, A.J. Thom, and M. Akinc. “Oxidation behavior of multiphase Nb-Mo-Si-B intermetallics.” *Metall. Mater. Trans. A*., 2005, vol. 36, 601-607.

[45] B. Portillo and S.K. Varma. “Oxidation behavior of Nb-20Mo-15Si-5B-20Ti alloy in air from 700 to 1300^{o}C.” *Journal of Alloys and Compounds*, 2010, vol. 497, 68-73.

[46] H.J. Grabke and G.H. Meier. “Accelerated oxidation, internal oxidation, intergranular oxidation, and pesting of intermetallic compounds.” *Oxidation of Metals*, 1995, vol. 44, 147-176.

[47] B.A. Pint, J.R. DiStefano, and I.G. Wright. “Oxidation resistance: one barrier to moving beyond Ni-base superalloys.” *Mater. Sci. Eng. A.,* 2006, vol. 415, 255-263.

[48] Pandat^{TM} 8.2. *Phase diagram calculation software for multicomponent system*s. CompuTherm LLC: Madison, WI 53719, 2009.

[49] H. Zheng, S. Lu, Z. Jianye, and L. Guangming. “Effect of Al additions on the oxidation behavior of laves phase $NbCr_2$ alloys at 1373K and 1473K.” *Int. Journal of Refractory Metals and Hard Materials*, 2009, vol. 27, 659-663.

[50] E.S.K. Menon, M.G. Mendiratta, and D.M. Dimiduk. “Oxidation behavior of complex niobium based alloys.” Niob. Scien. Tech., 2001, 121-145.

[51] J. L. Waring, R.S. Roth, and H.S. Parker. Res. Nat. Bur. Stand., 1973, vol. 77A, 705.

CURRICULUM VITAE

Alma Vazquez was born in Mexico City, Mexico, on February 11, 1985. She relocated to Ciudad Juarez, Chihuahua when she was three years old. She majored in Metallurgical and Materials Engineering at The University of Texas at El Paso. She obtained her B.S. in December 2008. Alma continued to study her masters at the University of Texas at El Paso in the Department of Metallurgical and Materials Engineering. She did research on high oxidation temperature of Nb-based alloys. She attended and presented a part of her research at the MS&T 2010 conference in Houston, Texas.

Permanent Address: 535 S. Mesa Hills #624

El Paso, TX, 79912

This thesis was typed and prepared by the author